TRIBHUVAN UNIVERSITY
INSTITUTE OF ENGINEERING
PULCHOWK CAMPUS

THESIS NO: 076/MSPSE/005

Tracing Synchronous Generator's Capability Curve for Better Visualization of Its Operating Condition

by

Bimal Gyawali

A THESIS
SUBMITTED TO DEPARTMENT OF ELECTRICAL ENGINEERING IN PARTIAL FULFILLMENT OF THE REQUIREMENTS FOR THE DEGREE OF MASTER OF SCIENCE IN POWER SYSTEM ENGINEERING

DEPARTMENT OF ELECTRICAL ENGINEERING
LALITPUR, NEPAL

SEPTEMBER, 2022

COPYRIGHT

TRIBHUVAN UNIVERSITY

INSTITUTE OF ENGINEERING

PULCHOWK CAMPUS, LALITPUR

DEPARTMENT OF ELECTRICAL ENGINEERING

The undersigned certify that they have read and recommended to the Institute of Engineering for acceptance, a thesis entitled "**Tracing Synchronous Generator's Capability Curve for Better Visualization of Its Operating Condition**" submitted by Bimal Gyawali in partial fulfillment of the requirements for the degree of Master of Science in Power System Engineering.

Professor Dr. Nava Raj Karki

Supervisor & Program Coordinator

MSc. In Power System Engineering

Department of Electrical Engineering

Pulchowk Campus, Lalitpur

Assoc. Prof. Dr. Bishal Silwal

External Examiner

Department of Electrical and Electronics Engineering

Kathmandu University, Kavre

Assoc. Prof. Mahammad Badrudoza

Department Head of Electrical Engineering

Pulchowk Campus, Lalitpur

September, 2022

ABSTRACT

The operation of both new and existing synchronous machine power plants must take into account entirely new requirements as a result of the quicker shift to renewable energy sources. Capability diagrams are essential for assessing synchronous machines' efficiency and operating ranFtge under various loading conditions. Also, change of machine parameters due to magnetic saturation may cause the originally provided capability curve insufficient to obtain an accurate operating region. The study presented in this thesis work fulfils the need for actual visualization of capability diagrams using the MATLAB software environment for both cylindrical and non-cylindrical rotor type synchronous machines.

Initially, the capability curve of machines is plotted considering the limiting conditions and after that the simulation and study of variation on the PQ loading after occurrence of possible disturbance scenarios on the power system network is carried out in PSAT (Power System Analysis Toolbox) software. The Generator capability curve is developed in MATLAB software environment for both cylindrical and non-cylindrical rotor type machines and from the data obtained after time domain simulation in PSAT applied on an IEEE 9 and 14 bus power system the operating scheme of one round rotor generating unit of each test system is discovered in developed diagram. From the simulation studies, the changes are observed in bus voltages along with the operational shift of the generator based on various events. Besides, the reactive power generation alteration with the tap position of the generating transformer is studied.

ACKNOWLEDGEMENT

First and foremost, I would like to express my heartfelt gratitude to my thesis supervisor professor Nava Raj Karki, Department of Electrical Engineering, IOE Pulchowk Campus, for his insightful guidance and continuous supervision for the progress of this work. I would also like to express my sincerest thankfulness to the lecturers/professors and Department of Electrical Engineering, Institute of Engineering, Pulchowk Campus. This work would not have seen the light of the day without their support. Also, I am greatly indebted to Dr. Nirmal Paudel, Mr. Shahabuddin Khan and Mr. Pashupati Raj Gautam for their suggestions and constructive criticisms for the betterment of the work.

I am also grateful to Mr. Mahesh Bashyal, who tirelessly assisted me in the research and through fact-checking and rechecking the manuscript of the report.

My sincerest thanks also go to Mr. Ganesh Bhandari, who had been a great help throughout the study. By presenting solutions for challenges during study, he has constantly helped to expand the horizon of the study and help incorporate new perspectives in this research work.

I am also thankful to my colleagues, who lend a hand during the study, and the people who have willingly helped me out with their abilities, without their consistent support and encouragement, I would not have been able to advance at this rate.

Bimal Gyawali

September, 2022

TABLE OF CONTENTS

LIST OF FIGURES

LIST OF TABLES

LIST OF ABBREVIATIONS

Abbreviation	Full Form
AVR	Automatic Voltage Regulator
d-axis	Direct Axis
DC	Direct Current
DG	Distributed Generation
EMF	Electromotive Force
GCC	Generator Capability Curve
GUI	Graphical User Interface
HV	High Voltage
LTC	Load Tap Changer
OCC	Open Circuit Characteristics
OPF	Optimal Power Flow
PMU	Phasor Measurement Unit
PSAT	Power System Analysis Toolbox
q-axis	Quadrature Axis
RPC	Reactive Power Capability
SCC	Short Circuit Characteristics
SCR	Short Circuit Ratio
SG	Synchronous Generator

LIST OF SYMBOLS

Symbol	Name
A_{satu}, B_{satu}	Saturation factors
c	Arbitrary constant
E01	EMF
Eg	Induced voltage
Eg_{satu}	Saturated induced voltage
Iar	Armature current
k	Arbitrary constant
n	Number
P	Active power
pu	Per unit
Q	Reactive power
S	Apparent power
$S_{1.0}$, $S_{1.2}$	Saturation factors
t	Time
V	Voltage
Vtr	Terminal voltage
Xad	Armature reactance
Xd	Direct axis reactance
Xp	Potier reactance
δ	Rotor angle
I_{fid}	Saturated field current

CHAPTER 1:INTRODUCTION

1.1 Background

The worldwide energy scenario is perceiving the transition in the energy sector after the rapid increment in the variable renewable energy resources penetration on the existing grid. To further enhance the integration of renewable energy sources to the electricity grid it must take advantage from the larger operating range of synchronous machines. Both future and current generators will need to operate under conditions that are far different from those for which they were planned in order to accommodate operational flexibility [1].

The share of power generation by renewable resources excluding hydro attained 13% of the global energy in the year 2021 [2], greater than nuclear energy's share. The system is impacted by the rising use of distributed generation (DG) on the grid. In order to overcome the rapid ramping on the generation from the intermittent sources, more flexible operation of conventional power plants including hydropower is essential [3].

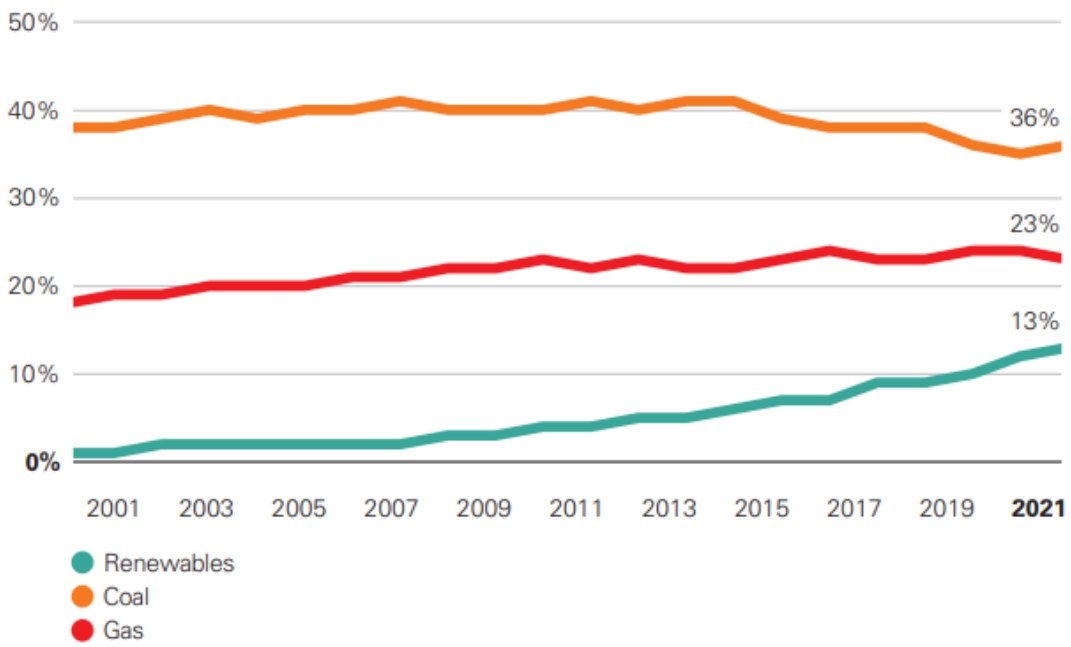

Figure 1-1: Increasing trend of renewable sources in global power generation [2].

In addition to the requirement of flexibility in operation, reactive power demand of the system is also extended as the share of renewables is growing. The conventional power

plants, like hydroelectric generators, are forced to enlarge their operational range as to incorporate the integration of renewable energy sources. In order to study the flexibility, the generator's capability diagram allows for more accurate observation of the synchronous generators' operational regimes.

Considering the fact of continuous increment of intermittent source, the conventional plants energy share is still dominating the power market. As long as the synchronous machines generated power plays an important role in the global energy mix, the enhancement in the operation of those plants is required for more flexible and reliable operation in the power system. The real operating condition of the power plant is required for the effective energy trade which is shown by the capability curve of the synchronous generator. Both thermal and hydropower plant's synchronous generator require the operating range by altering the machine parameters. The thermal generators support thermomechanical stresses while hydro generators that can also endure quick load ramping [4].

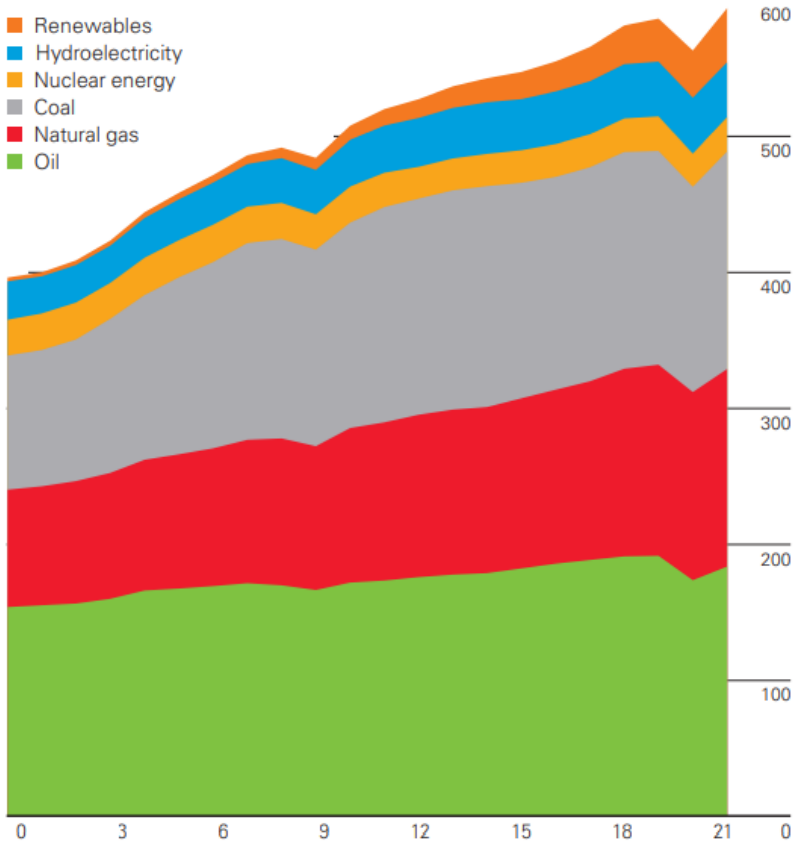

Figure 1-2: Sources of world energy consumption share [2].

The presented issues show the need for additional study in the operation of synchronous generators to determine the user-based capability chart for the visualization of the real operating range of the synchronous generator. Also, the active and reactive power regulation during the operation of the generator is important for the stable operation of the power plants and grid.

Due to the energy transition, current power system requires more flexibility, security and stability. Besides the optimal operation of the generating unit, safe operation is equally important for the long run of the unit without any disturbances [4]. A continuous matching between the energy supply to the prime mover and the electrical load on the system, as well as an adequate reactive power support mechanism to keep voltage within limits at different buses, is required for the stable operation of the power system. It is observed that the active and reactive power support that a generator can offer to the network can be significantly different from the value indicated by the standard generator capability curve provided by the manufacturer at the time of the generator's commissioning [5].

Due to the aging and variation in the operating environments the machine’s parameters differ from the previously obtained value. Although the generator aging is not considered in this thesis work, the effect of magnetic saturation in the capability chart is visualized. The visual tool to develop the synchronous generator capability chart by manipulating the machine’s parameters is necessary for the machine operators and load dispatchers to observe the operating area changes. It is required to get familiarized with all the possibilities of synchronous generators in order to obtain the technical and economical benefits to the electric power system. The synchronous generators capability diagram depicts the operating regions based on which other technical and economical aspects could be analysed. It is not possible to know the actual possibilities in the synchronous generators while using the standard capability diagram. The real environment-based capability diagram can provide the real working range of the synchronous generators. The actual depiction of a generator's capacity curve can replicate the generator's operating condition while taking into account the limitations of the generator's numerous constraints [4]. When the generator operates on the grid, with varying system parameters the limitations on the capability curve vary by some

extent which shows the need for the virtual realization of operational limits of the generator to make sure that the synchronous generator is used more efficiently.

The synchronous generators capability diagram is an essential component of a connected power system, to determine a generator's ability in supplying real and reactive powers. The operation of a generator is limited by the range considering the safety of the equipment. The protecting devices settings are made based on the operation limits to reduce the risk of damage to the equipment and power components during any type of disruptions. In order to achieve the proper functioning of the synchronous machine, the operating points need to be coordinated with the capability curve [8]. The stator heating limit, field heating limit, stator end heating limit, and turbine capacity limit are shown on the generator capability diagram as constraints on the unit's operation [7]. The generator will be able to operate without exceeding their thermal limits due to the actual parameter-based capability diagram. The actual depiction of the capability diagram will guide the generator's proper operation and aid in the investigation of voltage stability, including the dynamics of Load Tap Changer (LTC) with the Generator Capability Curve (GCC) can assist the electric utility for voltage support.

Recently, voltage stability is taken with higher priority for the appropriate operation of the power system and a synchronous generator plays a vital role in maintaining stability in the system. Several occurrences of voltage collapse have been recorded in various parts of the world [6]. The main cause of voltage instability is the power system's failure to supply the reactive power demand in an electrical network. During voltage concerns, generators are often the source of reactive power support. One of the most significant countermeasures for voltage collapse is to monitor voltage profiles, voltage regulation, and generator reactive power output.

This thesis work is concerned with the calculation of magnetic saturation of the salient pole machine and determination of capability chart for both salient-pole and non-salient pole machines utilizing MATLAB for computation and results. Besides, it also gives the insights to the operating condition of the synchronous generators of the power system network during the occurrence of contingencies and its representation into the PQ diagram. The study of the operating scenarios of the generators assists power system

operators to decide the countermeasures for the real and reactive power balance within the system. Additionally, the effect of on load tap changer on the reactive power output of the generating unit is also depicted in this work.

1.2 Problem Statement

The bounds for supplying reactive power at a particular active power output are determined by the generator capability diagram or generator performance chart issued by the manufacturer at the time of unit commissioning. The assumption of constant direct-axis synchronous reactance is incorrect since synchronous machines are designed with a certain amount of saturation and are affected by machine operating parameters such as armature voltage and current. Even if the generator itself is completely safe, crossing these limitations may result in violations of numerous constraints imposed by other equipment and events in the power system. The post-disturbance scenario analysis is required in the system to plan for the countermeasures for those events. The better approach of load dispatch is required considering the real operating limits [5] to provide more effective voltage control of the high-voltage grid during contingencies.

Moreover, the need for flexibility in the utility due to the intermittent nature of sources like solar and wind, is required to ensure there is enough rotating mass and to create flexible functioning. A continuous matching between the energy supply to the prime mover and the electrical load on the system is required for stable power system operation, as an adequate reactive power support mechanism is required to keep voltage within limits at different buses. At the moment, dispatchers rely on manufactures provided capability diagram which is not realized in the real working environment by altering the machines parameters. To accumulate the changes in the machine's working condition power plant operators require the real-time operation regimes of the power plant to improve availability, particularly in the event of an emergency [14].

1.3 Objectives

1.3.1 Main objective

The main objective of this thesis work is to graphically visualize the synchronous generator's capability diagram and disturbance scenario analysis on test system based upon the parameters obtained from simulation.

1.3.2 Specific objectives

The specific objectives of this study are:

- To model a comprehensive visual depiction of the capability diagram incorporating all the constraints governing it in the MATLAB.
- To determine the operating point in capability curve and fluctuation in bus voltage during normal and disturbance situations.
- To perform the magnetic saturation calculation of the salient pole synchronous generator.

1.4 Scope of the work

Using time-domain simulations, the disturbance scenario on bus voltage will be investigated using a conventional IEEE 9 bus test system and IEEE 14 bus test system. In addition, a software tool will be developed to visualize the generator's capability curve for both salient pole and non-salient pole synchronous machines.

1.5 Limitations

Following are the limitations of the proposed study:

- The infinite bus-bar assumption will be considered during implementation, which is not practicable in the actual world because the terminal voltage can fluctuate greatly from the rated value.
- The thermal ageing of the generator and temperature visualization is not inclusive in this work.

CHAPTER 2:LITERATURE REVIEW

A synchronous generator is made up of two windings: stator winding and rotor winding. The rotor winding generally consists of two types: salient pole and non-salient pole construction. The rotor winding receives a direct current (DC), which creates a magnetic field in the rotor. A prime mover (such as steam, water, etc.) then turns the rotor, creating a rotating magnetic field. The generator's stator windings experience a three-phase set of voltages as a result of this rotating magnetic field.

2.1 Relevant Theory

2.1.1 Short Circuit Ratio

A generator's short circuit ratio (SCR) measures how well it can deliver a short circuit current to its terminals. A power system's short circuit capabilities are closely tied to the grid architecture and short circuit characteristics of its power generation [1]. Equation 2.1 gives the expression of the short circuit ratio. In other words, it is the ratio of the field current needed to produce the rated armature voltage at open circuit to the field current needed to produce the rated armature current at short circuit [6].

$$SCR=\frac{IF_{oc}}{If_{sc}} \qquad \text{Equation 2.1}$$

The synchronous reactance in the d-axis decreases with increasing SCR. This implies that a power system has a strong grid if the SCR is greater than 1 [1]. As a result, the generator will be less susceptible to frequency changes and be able to produce more short circuit current. In order to increase the stability of the machine while it is connected to the grid, the SCR value for hydraulic units is typically higher than that for thermal generators. However, this will also result in a higher short circuit current delivery capability for the machine, which will increase machine size and cost.

The short circuit ratio and the reactive power capability (RPC) are closely related. A high SCR considerably improves the RPC [7]. This is so that the generator's internal parasitic reactive power consumption is decreased by the high SCR's reduction of the d-axis synchronous reactance Xd. If the magnetic saturation is calculated, a dynamic

SCR can be essential for improved RPC, for wider reactive power operating range considering the intermittent sources.

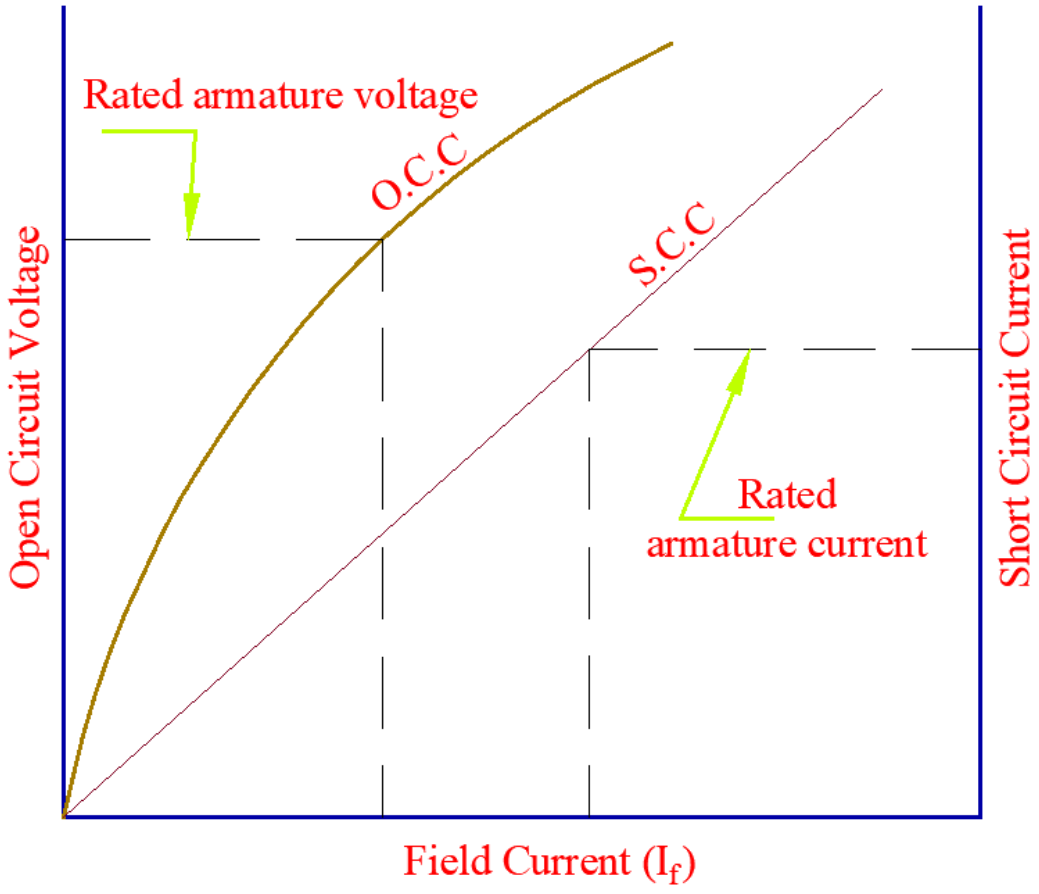

Figure 2-1: OCC and SCC curve of synchronous generator.

2.1.2 Infinite Grid:

The generator is a part of an infinite grid. This demonstrates that the circuit's voltage is constant and set at 1 pu. Given the values of 1 pu and 0 degrees, the generator terminal is selected as the reference point. This also implies that the armature current and apparent power are directly related. This is demonstrated in Equation 2.2.

$$I_{ar} = \frac{S}{E01} = \frac{\sqrt{(P^2+Q^2)}}{1}$$ Equation 2.2

2.1.3 Synchronous Reactance:

The voltage effects in the armature circuit induced by the actual armature leakage reactance and by the change in the air gap flux generated by the armature reaction are accounted for by imagined synchronous reactance. For the examination of a generator's operation, control, maintenance, and performance, knowing all of its precise parameters is crucial. Over time, some generator parameters might change as synchronous reactance could be changed due to magnetic saturation [8]. The deterioration of the generator's magnetic properties is the primary cause of changes.

2.1.4 Synchronous Machine Magnetic Saturation

A phenomenon known as saturation occurs when the values of y in a functional or physical relationship such as y = f(x) no longer significantly vary for sufficiently large x. Magnetic saturation occurs when a large number of the magnetic domains align, and the introduction of a magnetic field no longer creates a considerable rise in magnetic intensity. According to Reference [9], the most crucial element in the development of synchronous machine models is saturation representation. Saturation and other modeling techniques are taken into account in paper [1], as well as in academic book [6]. A representative saturation curve for a synchronous generator is shown in Figure 2-2.

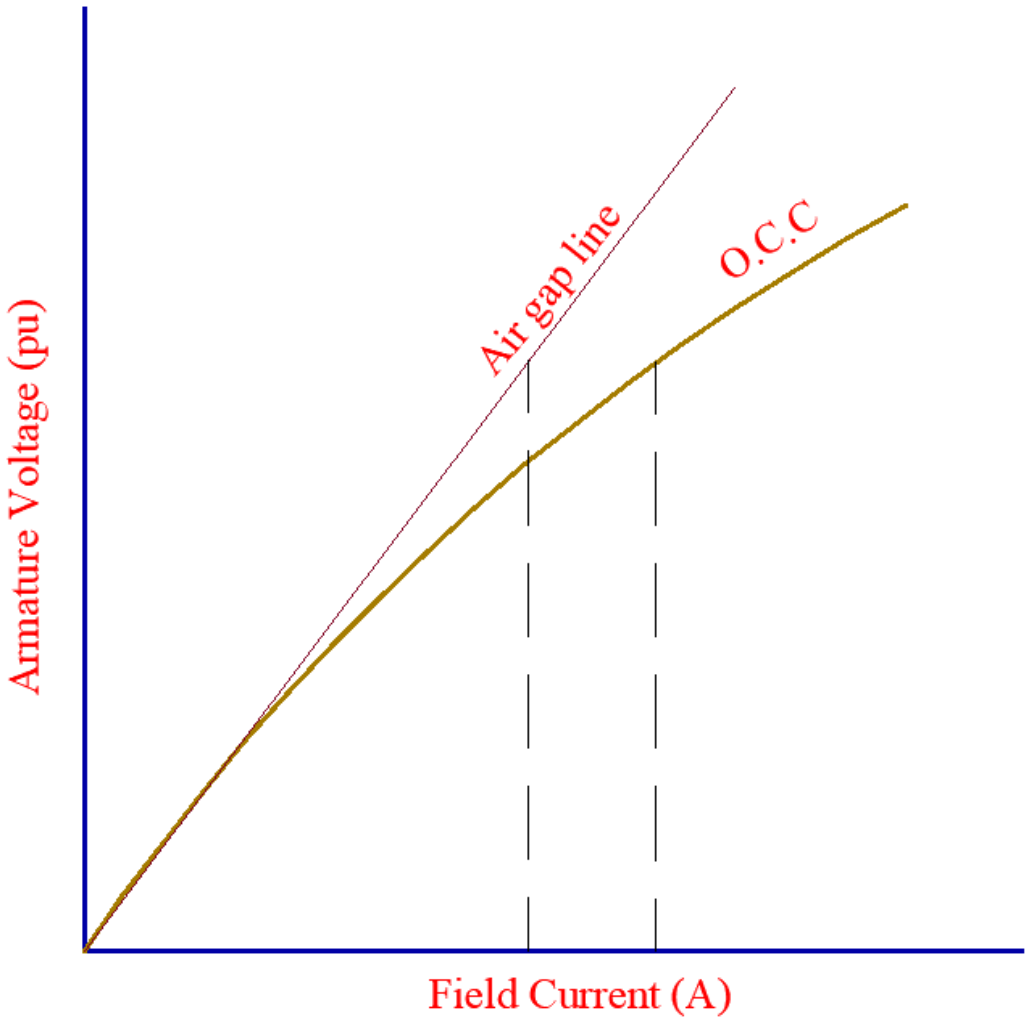

Figure 2-2: Visual representation of saturation curve.

Among different existing saturation calculation models Anderson and Fouad have proposed a superior approach in [10]. An exponential form has been proposed by them. The coefficients were determined using data for 1.0 and 1.2 p.u. voltages. As the non-linear saturation properties can be accurately reflected by adjusting the saturation factor, the Anderson and Fouad technique is accurate to measure the saturation level [3]. The disadvantage is that calculating the saturation factors takes time.

2.2 Capability Diagram

A synchronous generator's operational limit is mostly thermal in nature. The machine heats up as a result of the current going through the windings. Of course, the machine is built to tolerate this temperature increase as long as it operates in a permitted area.

The capacity chart defines an area where the machine can operate freely without exceeding temperature restrictions in the geometric locus of active and reactive power planes. Excellent advice on how to draw the capability chart may be found in references [3] to [11].

Generator's capability curve offers an effective tool for electrical generator loading and to visualize the generator's operating limits. They are utilized to load the synchronous generators under various operating circumstances without going above the predetermined limitations. Manufacturer also provides capability curves in standard condition. The capability curves' most significant representation in the two-dimensional plane include steady state stability, stator and rotor current limits, and thermal constraints [11].

2.2.1 Equivalent Synchronous Generator Circuit

The voltage E01 is the internally generated voltage created by a synchronous generator's one phase. The machine's terminal voltage Vtr will be equal to the voltage induced at the stator coils if there is no load attached to it (no armature current flowing). This is because there are no losses because there is no current flowing through the stator coils. There will be variations between E01 and Vtr when the generator is connected to a load. These variations result from:

- The distortion of the air gap magnetic field caused by the stator's current flow (armature reaction).
- The armature coil's self-inductance
- The armature coils' resistance
- Salient pole rotor shapes' impact.

Consider the model below as a cylindrical rotor generator connected to any load.

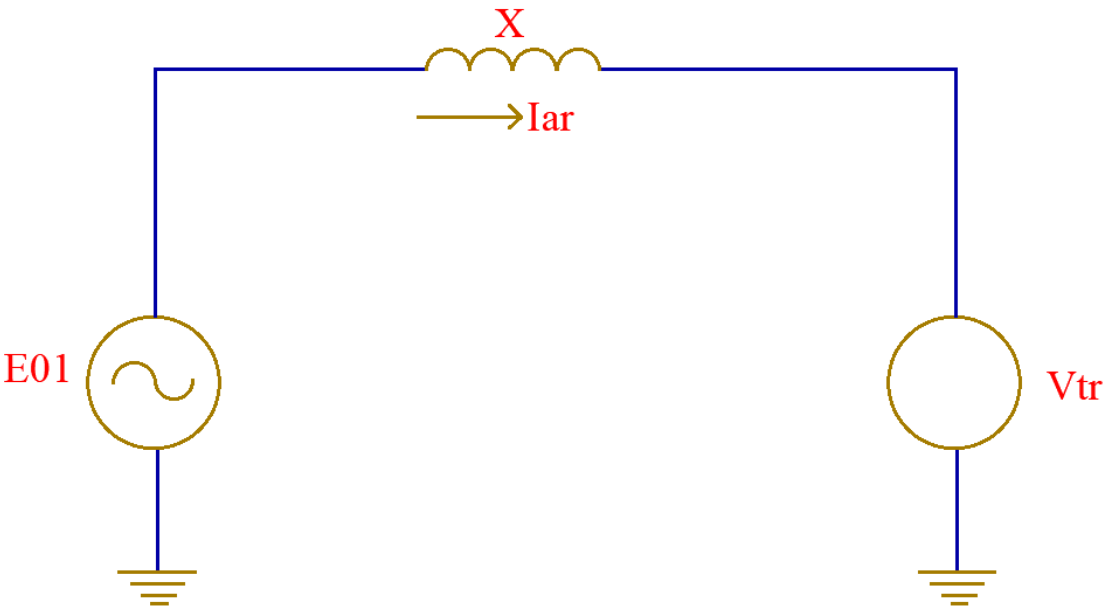

Figure 2-3: Equivalent circuit diagram.

If Iar is the load current, X is the machine reactance, E01 is the induced voltage, and Vtr is the terminal voltage. When the saliency of a machine is neglected for cylindrical or round rotor machines Xd=Xq=Xs=X. The following expression can be written for an inductive load using the terminal voltage as a reference.

$$E01=Vtr+jIarX \qquad \text{Equation 2.3}$$

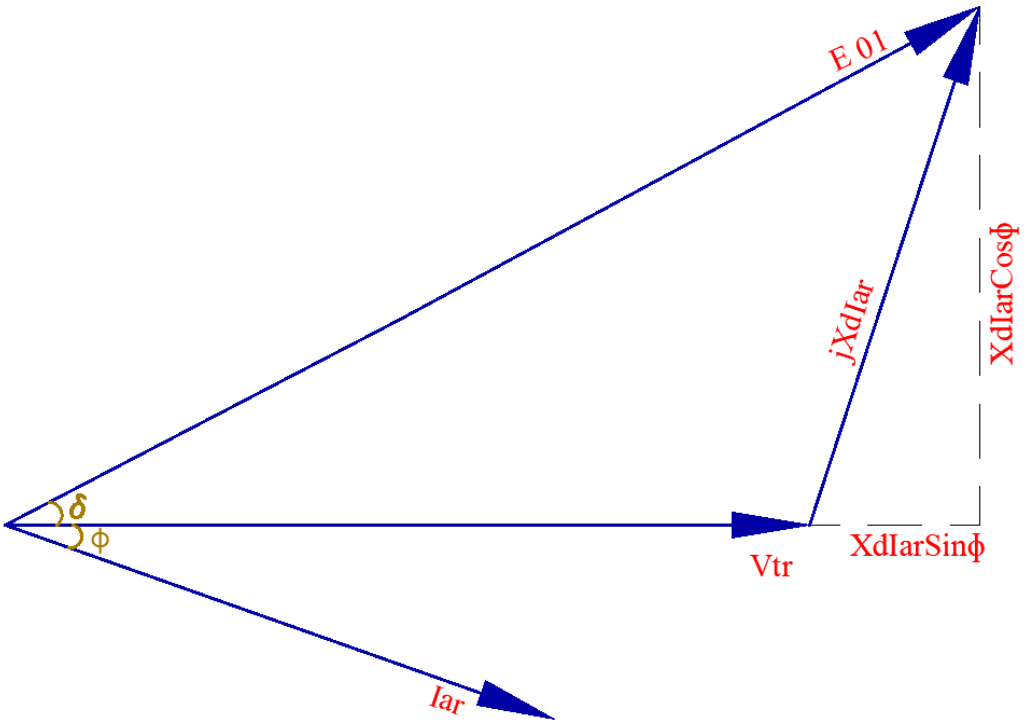

Figure 2-4: Phasor depiction of equivalent diagram.

The current flowing through X or Xd is given by:

$$I_{ar}=\frac{E_{01}-V_{tr}}{jXd} \qquad \text{Equation 2.4}$$

Where E01 is the constant emf behind reactance and Vtr is the terminal voltage. The apparent power from the sending end is:

$$S=V_{tr}I_{ar}^{*} \qquad \text{Equation 2.5}$$

$$\text{or, } P+jQ=\frac{E_{01}V_{tr}\sin\delta}{Xd}+j\frac{E_{01}V_{tr}\cos\delta-V_{tr}^{2}}{Xd} \qquad \text{Equation 2.6}$$

The real power at sending end is:

$$P=\frac{E_{01}V_{tr}\sin\delta}{Xd} \qquad \text{Equation 2.7}$$

The reactive power at sending end is:

$$Q=\frac{E_{01}V_{tr}\cos\delta-V_{tr}^2}{Xd}$$ Equation 2.8

where,

Xd = direct axis synchronous reactance.

E01 = electromotive force (emf) of air-gap.

Vtr = terminal voltage.

δ = load angle of generator.

This diagram shows the δ angle. This angle is generally termed as the power or load angle. The angle between induced and terminal voltages, not the load angle, determines the load power factor.

2.2.2 Phasor diagram

The synchronous machine described above is only viable for machines with cylindrical rotors when it is represented as a reactance behind a power supply model. As a round rotor generator's reluctance is nearly constant no matter which direction it is pointed. But, in case of salient pole machine the direct axis reactance and the quadrature axis reactance are two different types of reactance because the reluctance is significantly smaller in the pole shoe region (direct axis) than in the region between the poles (quadrature axis) [3]. In salient pole machines, the quadrature axis reactance (Xq) typically ranges from 65% to 85% of the direct axis reactance (Xd), but for round rotor machines, it ranges from 92% to 98% of the direct axis reactance validating the Xd~=Xq [3].

Consider the model below as a non-cylindrical rotor generator connected to any load.

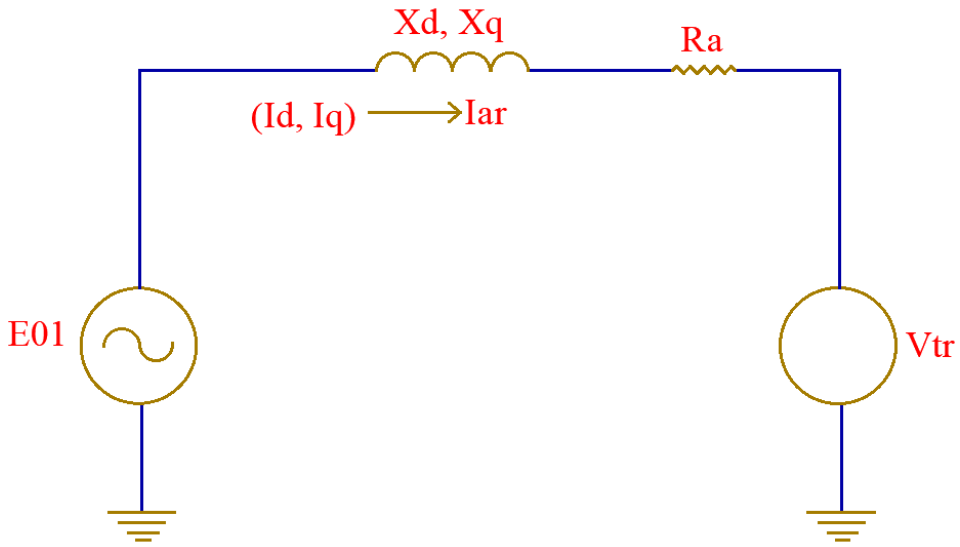

Figure 2-5: Equivalent circuit of salient pole generator.

If Iar is the load current, X is the machine reactance, E01 is the induced voltage, and Vtr is the terminal voltage. The following expression can be written for an inductive load using the terminal voltage as a reference and considering Ra<<X to neglect the effect of armature resistance for salient pole machines.

$$E01 = Vtr + jIXdId + jXqIq \qquad \text{Equation 2.9}$$

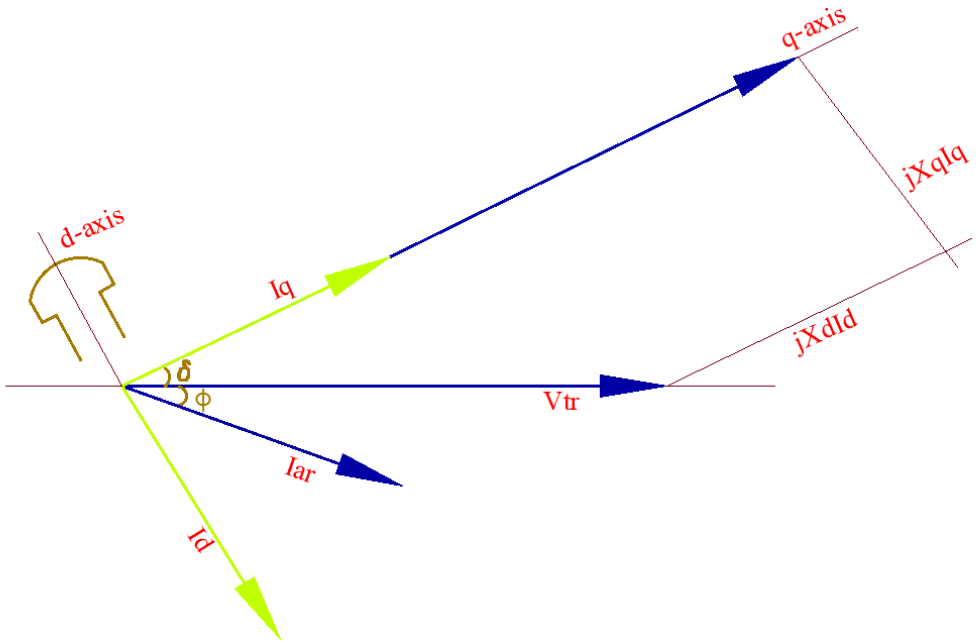

Figure 2-6: Phasor diagram of salient pole machine.

The above obtained phasor diagram can be simplified in more representable form by introducing mathematical artifice, jXqId is added and subtracted as the previous phasor diagram is difficult to obtain while the d- and q-axis locations are uncertain [3].

$$E01=Vtr+ jIXdId + jXqIq + jXqId – jXqId \quad \text{Equation 2.10}$$

$$\therefore E01=Vtr+j(Xd-Xq)Id+jXqI \quad \text{Equation 2.11}$$

From Equation 2.11, the following phasor diagram can be obtained.

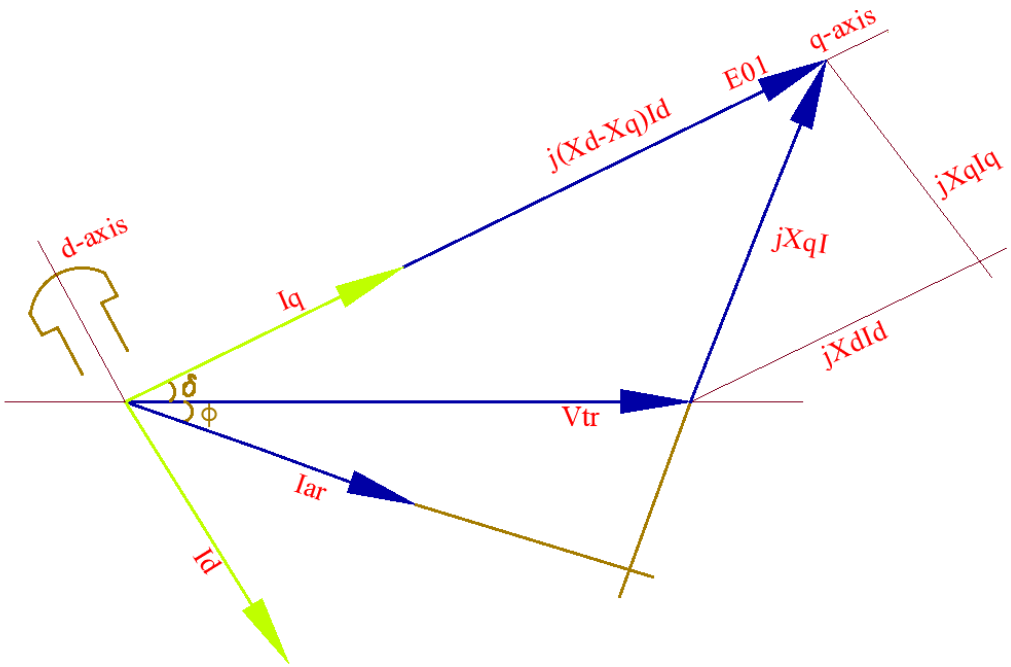

Figure 2-7: Modified phasor diagram of salient pole machine.

From the above phasor diagram, the generated active and reactive powers for a salient pole machine can be estimated using Equation 2.12 and Equation 2.13 respectively.

$$P=\frac{E_{01}V_{tr}}{X_d}\sin\delta+\frac{V_{tr}^2}{2}\left(\frac{1}{X_d}-\frac{1}{X_q}\right)\sin(2\delta) \quad \text{Equation 2.12}$$

$$Q=\frac{E_{01}V_{tr}}{X_d}\cos\delta-V_{tr}^2\left[\frac{\sin^2(\delta)}{X_d}+\frac{\cos^2\delta}{X_q}\right] \quad \text{Equation 2.13}$$

2.3 Steady State Operation

A synchronous generator's steady state functioning involves controlling the frequency and effective value of the terminal voltage when it is out of synchronism. When a machine is connected to a power system that is considered as an infinite bus, the power system determines both the frequency and voltage. The voltage regulator and speed governor in this situation fail to accomplish their primary objectives and are now in charge of distributing active and reactive power. The functions of the regulator under a grid-connected scenario are shown in the following table.

Table 2-1: Regulation of power system components.

Component	On-grid Operation
Speed governor	Active power
Automatic voltage regulator	Reactive power

2.4 P-δ diagram

The generated active power is substantially correlated with the power angle and less correlated with the induced voltage, as shown by Equation 2.7 and Equation 2.12. On the other hand, as shown in Equation 2.8 and Equation 2.13, the reactive power is substantially reliant on the induced voltage and less dependent on the power angle. It could be explained by the fact that the cosine function exhibits the opposite behavior to the sin function, which has a large derivative near to zero.

Additionally, as can be seen in Equation 2.7, maximum round rotor generator's power transfer occurs at a loading angle of 90 degrees. Beyond this angle, the load angle increases, causing an instability process to start. As shown in Figure 2-8, the theoretical stability limit for round rotor machines is 90 degrees.

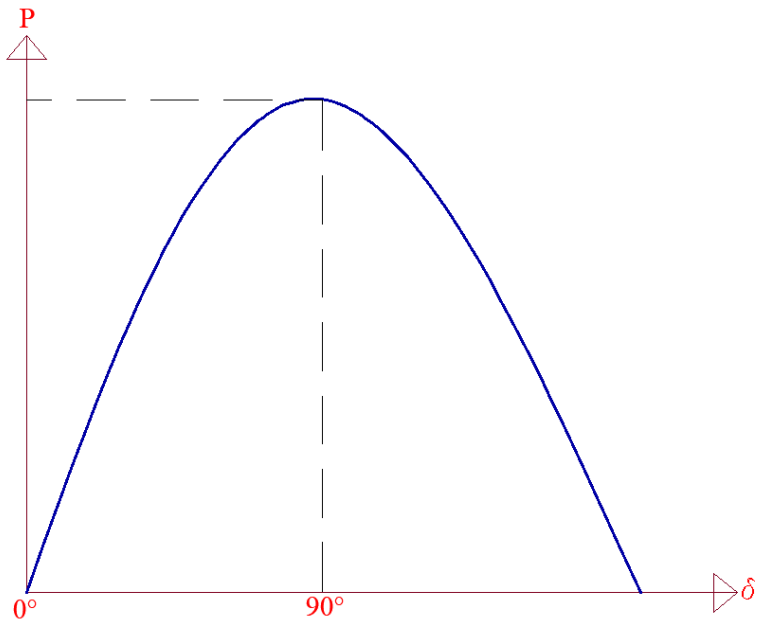

Figure 2-8: P-δ diagram of round rotor machine.

But, in case of salient pole machines the theoretical stability limit is less than 90 degrees. It is due to the second harmonic component known as "reluctance power". It results from the reluctance difference, which produces different types of reactance Xd and Xq [3].

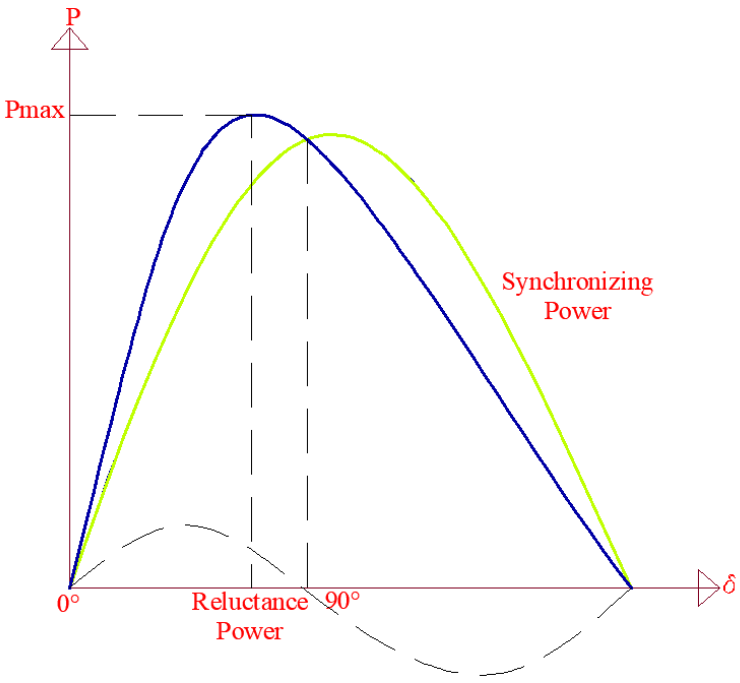

Figure 2-9: P- δ diagram of non-cylindrical rotor machine.

2.5 Construction of capability chart

The classical capability curve is formed by taking the generator terminal voltage as reference and by multiplying the voltage phasor diagram by current phasors to obtain the power phasor diagram as shown in Figure 2-10. The active power is denoted in vertical axis and reactive power is denoted in horizontal axis of the power phasor diagram as shown in Figure 2-10. The generator capability curve expresses and visualizes the generator operating point restrictions. Apparent power (MVA), active power (MW) and reactive power (MVAR) are all included in the generator load capability curve and generator operating capability. The MW and MVAr axis is used to represent the capability curve.

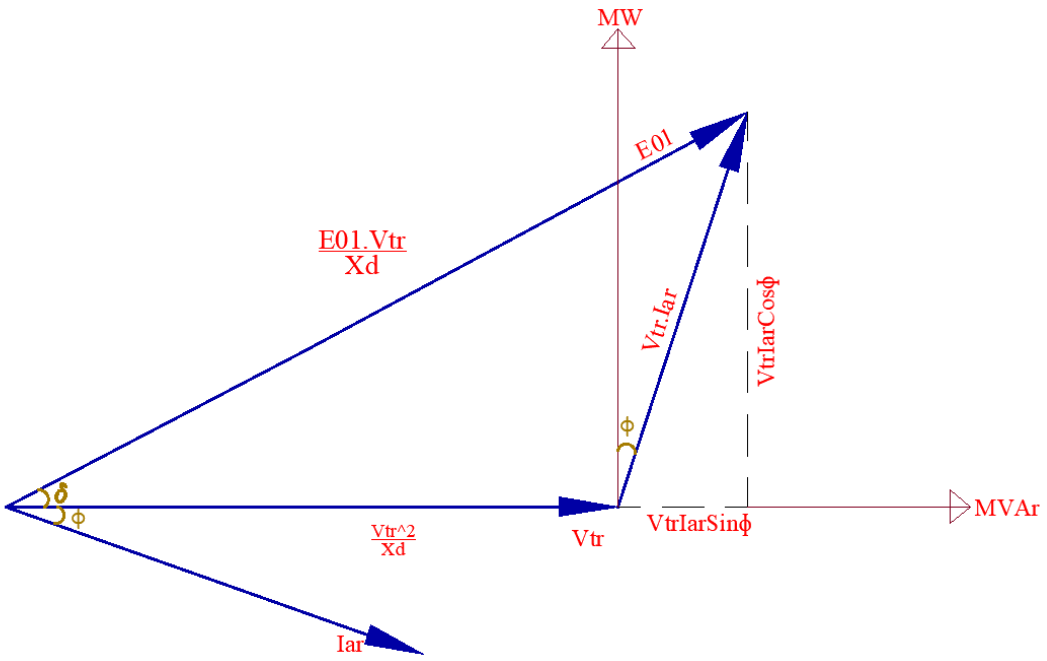

Figure 2-10: Steady state power phasor diagram.

A synchronous generator is an active and reactive power source that may be adjusted over a large range of values. An operating range that is safe for the generator to run in without going over its thermal limits is displayed in the generator capability diagram. Furthermore, the right settings of the relays employed in the protection of synchronous generators, such as automatic voltage regulator (AVR), overexcitation limiter, under-excited controllers and loss of field relay, are another vital role of the capability curves [12]. The limits of the capability chart of the generator are [9]:

- Rated field current limit.
- Rated stator/armature current limit.
- Rated output power of the turbine.
- Steady state stability limit.
- Stator end heating limit.

2.5.1 Field current limit

A continuous supply of field current is essential to produce a rotating magnetic field at the rotor. Because of the I_f^2 power loss, the field winding heats up [6]. So, in order to keep the temperature in field windings within a particular range, the field current I_f must be smaller than a certain maximum value, say I_f max.

2.5.2 Armature current limit

After the electromagnetic induction in the armature coil continuous current starts flowing through the stator windings. The armature current I_a creates a I_a^2R loss this armature winding power loss raises the winding temperature [6]. To keep the temperature rise to a minimum, this current should be less than a particular maximum value $I_a$max.

2.5.3 Steady-state stability limit

The load angle δ should be kept within the limit for generators to operate safely, and the theoretical stability limit is reached when δ= 90°. In reality, however, a safety range is always added to allow for a load increase of either 10% or 20% before instability [6]. At constant field current, the active power output can be decreased by 10% of the rated power in order to reach the realistic stability limit.

2.5.4 Generator active power limit

The turbine power limits the generator's active power, which varies depending on the kind of turbine. The two turbine limits, higher Pmax and lower Pmin, can be represented in the PQ plane by two lines parallel to the Q-axis though minimum limit is given low priority.

2.5.5 Stator end region heating limit

This limitation is caused by localized heating at the armature's end during under-excited synchronous generator operation. The retaining ring is not saturated during under-excitation operation because the field current is low, and the flux created by the armature current is added to the flux produced by the field current.

2.5.6 Capability diagram interpretation

Several parameters related to the operation of a synchronous generator can be identified from the capability curve. The active and reactive power, power factor, load angle, excitation current, and other parameters may be computed based on the generator's operating point, and the generator's stability can be evaluated. The operation in the inductive regime with production of reactive power is represented by the zone on the right side of the active power axis (MW-axis); the operation in the capacitive regime with absorption of reactive power is represented by the zone on the left side of the active power axis (MW-axis) [11]. The field current limit and the stator current limit are established by the requirement of not exceeding the permissible temperatures when operating in an inductive regime (over excitation). The extra electric losses in the frontal zone of the stator, as well as the static stability limit, influence operation in a capacitive regime (under excitation).

Thermal limits, which may result from currents flowing in the machine windings or from the circulation of eddy currents in the magnetic core of the armature, are the most severe operational restrictions that can be imposed on a specific machine. The geometric locus in the active and reactive power plane where the machine can operate freely without violating temperature limitations is, thus, identified by the capability chart. Stability is a further limit that needs to be taken into consideration.

The limits are indicated on a hypothetical capability chart for a non-salient pole synchronous machine in Figure 2-11. The rated armature current and rated power factor together with the part A–B represent the field heating limit. The rated apparent power, which is proportional to the rated armature current, defines B-C as the armature heating limit. When the saliency is ignored, Xq and Xd are equal. Consequently, the semicircle

shrinks into a single point. This Figure 2-11 also shows the armature core end heating limit mentioned in parts C-D, which is appropriate for machines with rounded rotors but neglected for machines with salient poles.

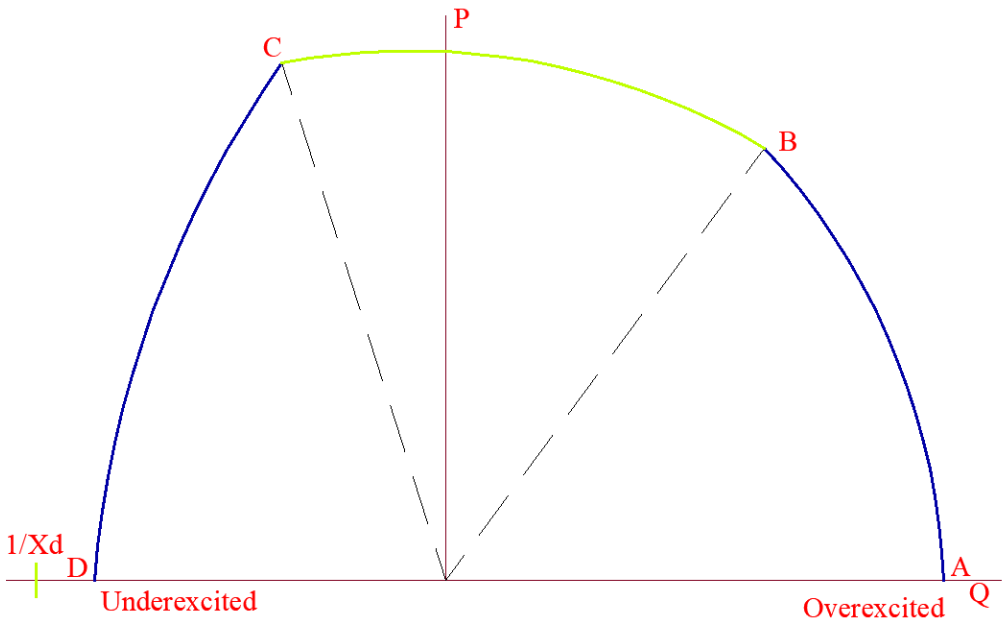

Figure 2-11: Capability curve of cylindrical rotor machine.

A salient pole synchronous machine's capability chart is shown in Figure 2-12. The capability chart of a round rotor synchronous machine can be compared to the parts A-B and B-C of this chart. The theoretical stability limit yields C-D, the practical stability limit, and D-E, the minimal field current, which is determined by the machine's residual magnetism.

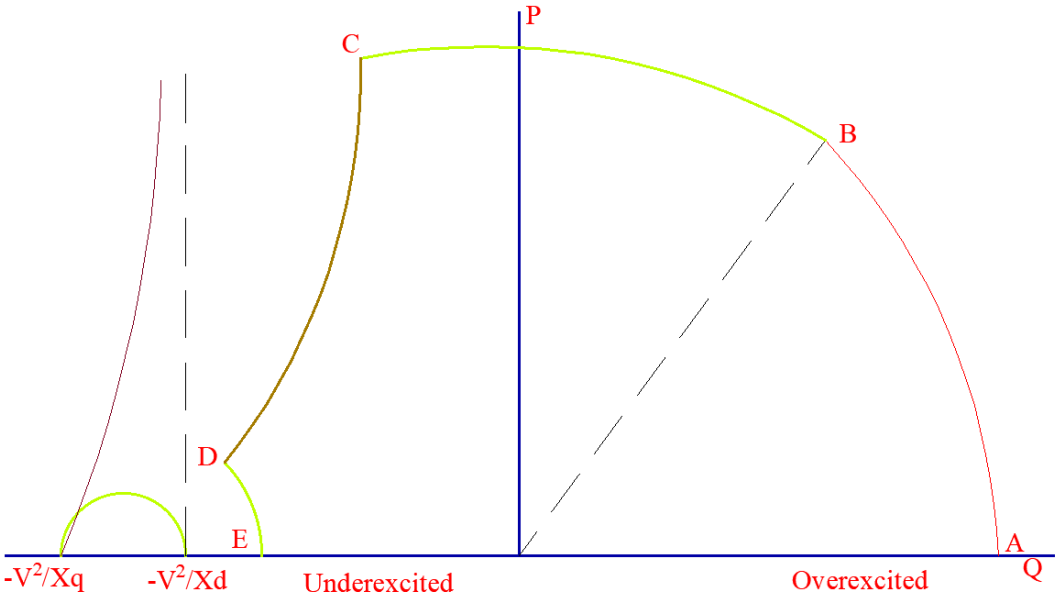

Figure 2-12: Capability chart of salient pole synchronous machine.

It is possible to overload the synchronous machine for a brief period of time without degrading the insulation for the time given by following Equation 2.14 [13].

$$t=\frac{k}{I^2-1} \qquad \text{Equation 2.14}$$

Where,

t= overloading time (s).

k= value provided by the manufacturer that ranges from 100 to 250.

I= overloading current (pu).

2.6 Voltage Stability

Voltage stability refers to a power system's capacity to maintain a constant, acceptable voltage across all buses during normal operating conditions and after being subjected to a disturbance [6]. Voltage instability arises in when the voltage drops uncontrollably due to system faults, loss of generators or lines, an increase in load demand, or a change in the state of the system. The main cause of instability is the power system's inability to meet reactive power demand.

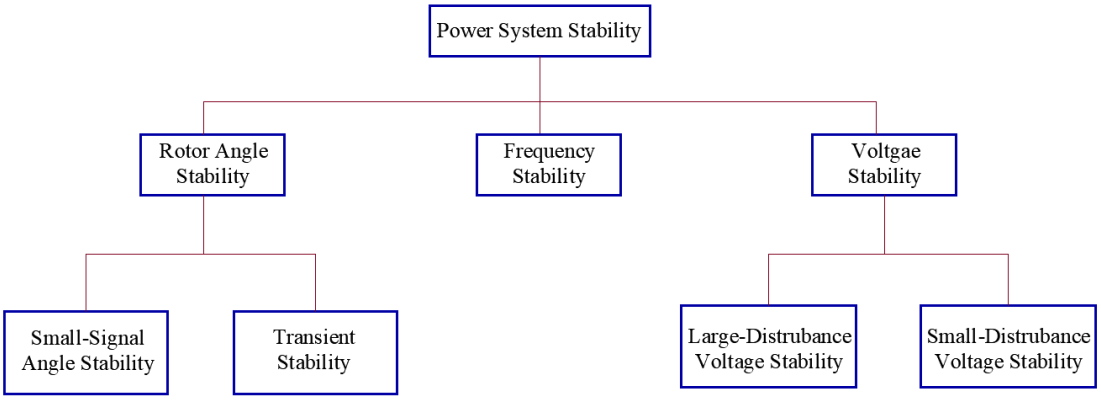

Figure 2-13: Classification of power system stability [14].

By identifying the maximum reactive power a system may deliver to a load, the system's voltage stability limit or margin, can be specified.

2.6.1 Voltage collapse phenomenon

Voltage collapse can take from around a few seconds to tens of minutes to occur. As a result, depending on how long dynamics last, there are basically two-time frames for voltage stability: short term and long term. Long-term voltage collapse is caused by slow-acting load elements like LTC transformers, thermostat-controlled loads, and generator excitation limiters.

2.6.2 Transformer load tap changer

A tap changer is a feature in transformers which enables for variable turn ratios to be adjusted in distinct phases. This is accomplished by connecting to a number of taps located along the primary or secondary winding. Under typical operating circumstances, as the reactive power (Q) supplied at the same bus is raised, so does the bus voltage magnitude (V). The system is considered to be unstable when the bus voltage magnitude (V) of any one of the system's buses declines while the reactive power (Q) for that same bus increases.

The voltage magnitude is set to 1.0 per unit and the indicated voltage variation limit is 5% in the Newton-Raphson load flow method. Therefore, the voltage magnitude (safe voltage limits) in system buses must be between 1.05 and 0.95 units. The voltage

magnitude at the system's weak locations is less than 0.95 [15]. The LTC transformer secondary voltage control method is depicted in Figure 2-14.

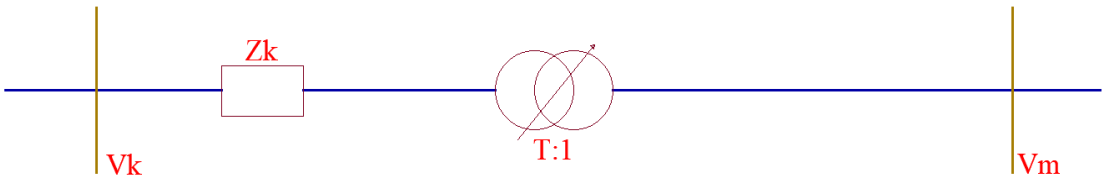

Figure 2-14: Secondary voltage control scheme of LTC transformer.

2.7 Consideration of the Disturbances

The standard approach for figuring out power transfer margins or the hazards associated with a change in loading conditions is contingency analysis. It makes it possible to decide what safeguards need to be put in place to avoid these dangers [16].The variations on the bus voltage and generator operational region is caused by a variety of faults in the network components.

2.7.1 Transmission Line Outage

The frequency and duration of various transmission line outages have a substantial impact on the operation and reliability of power networks [16].The outage in the transmission line adversely affects the nearby bus voltages.

2.7.2 Loads Variation

The variation on the loads may affect the load flow of the power system resulting in fluctuations in nearby bus voltages. The variations in load trigger disruptions in the nominal voltage profile. When the load increases, the voltage profile will drop, and when the load decreases, it will rise [17].

2.7.3 Faults in Bus-bar

Normally, the impact of bus bar faults depends on the type of fault and on the equipment connected to that point. The severity of fault depends on the fault clearing time, the

system remains stable only for momentary fault clearing time otherwise such faults may result in the unstable operation.

2.7.4 Generator Outage

Generator outage hampers the overall system parameters and if the system is unable to meet load instantly it may cause system collapse. The post-contingency voltage level is violated due to a lack of excess or reserve system power. Hence, the pre-contingency voltage series will be better than the post-contingency voltage level [17].

CHAPTER 3:METHODOLOGY

In this thesis work visualization of capability curves is done in a MATLAB software environment. For the round rotor machine, the generators of the test systems are considered. While for the capability diagram determination of salient pole machines a case study of Furnas hydropower as studied in [3] is considered. The magnetic saturation calculation is done in addition to the hydro-generator in order to visualize the change due to variation in saturated reactance.

Moreover, various disturbance conditions are applied to the test systems and the variation in the bus voltages are done. Furthermore, the change in reactive power output from the generator before and after the change in tap position is also observed.

3.1 Research workflow

The basic flowchart of this study is shown in Figure 3-1.

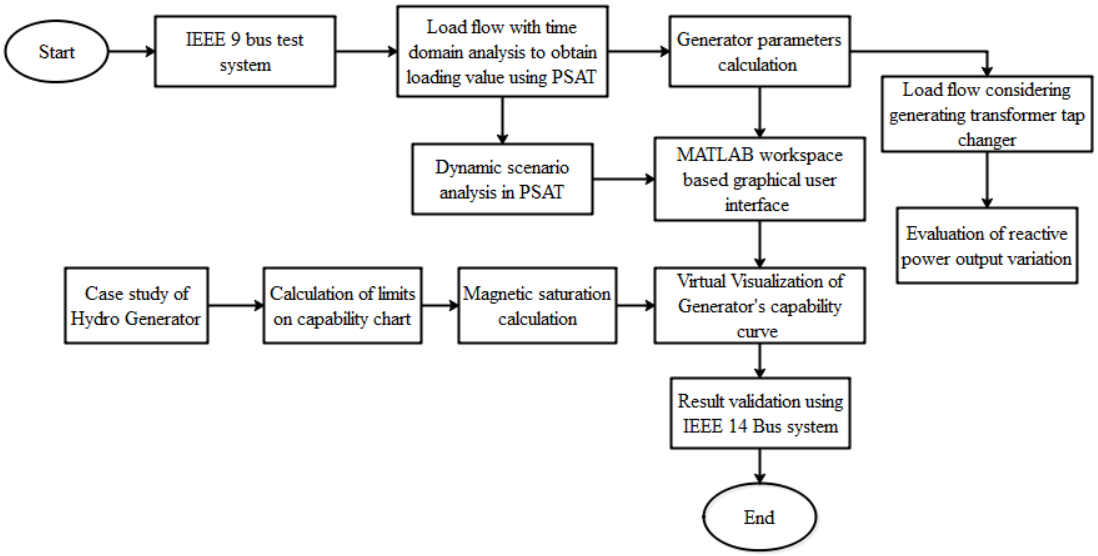

Figure 3-1: Workflow diagram of the study

3.2 Magnetic saturation calculation

The method utilized for saturation calculation in this research work is based on the Anderson and Fouad method as described in [10]. Saturation evaluation is a challenging task. kundur states in the book Power System Stability [6] that “Any practical method

of accounting for saturation effects must be based on semi-heuristic reasoning and judiciously chosen approximations, with due consideration to the simplicity of model structure, data availability, and accuracy of results".

In assessing the losses and the efficiency of the hydro generator at various loading points, the losses linked to the field current and magnetic saturation are considerably more important [1]. Before calculating the saturation, a number of assumptions need to be made. The primary presumption is listed below [6]:

- Leakage inductances are independent of saturation.
- Leakage flux does not contribute to the saturation of iron core.
- The resultant air gap flux and the mmf have the same saturation relationship under loaded and unloaded situations.
- Due to the non-linearities brought over by saturation, there is no magnetic coupling between the d-axis and q-axis.
- Due to the unavailability of load test, saturation is calculated using open circuit characteristics.

The open-circuit characteristics (OCC) can be shown in Figure 3-2. The induced voltage in the air gap is depicted in the figure as a function of the field current. For each operation, the saturation must be determined using the data that are currently accessible, so it is essential to choose a suitable approach and procedure. In this method the Equation 3.1 is used to fit the saturation curve.

$$I_{fid}=(V+C\times V^{n})\times k \qquad \text{Equation 3.1}$$

Where,

V= terminal voltage.

n= number either 7 or 9.

c= arbitrary constant.

k= arbitrary constant.

When the saturation is ignored, and the field current is directly proportional to the induced voltage. Equation 3.2 is used to generate the air gap line. When generators exhibit a linear property.

$$I_{fid}=E_g \qquad \text{Equation 3.2}$$

Where,

Eg= induced voltage.

When saturation is ignored, Equation 3.3 represents the armature reaction reactance.

$$X_{adu}=X_d-X_p \qquad \text{Equation 3.3}$$

Where,

Xadu= armature reactance.

Xp= potier reactance.

Only in the d-axis does saturation take place. This is as a result of the flux choosing the path with the least reluctance [6]. Because the d-axis air gap is substantially smaller than the q- axis, the reluctance is also much smaller. In other words, a salient pole generator's non-uniform air gap forces the flux to mostly pass through the d-axis.

The synchronous reactance in the d-axis Xd can be found by rearranging the Equation 3.3 provides an illustration of the synchronous reactance. The equation shows that saturation has an impact on both the synchronous reactance and the armature reactance.

$$X_d=X_{adu}+X_p \qquad \text{Equation 3.4}$$

According to the Anderson and Fouad approach, when the air gap line and the saturation curve are plotted, the procedure's subsequent step is followed to calculate out the saturation factor S. The saturation curve is computed by fitting the curve to obtain the proper slope. Regarding the OCC, a key assumption is that the properties of linear

saturation are discarded. This is due to the fact that this generator doesn't have an induced voltage that produces a linear saturation characteristic.

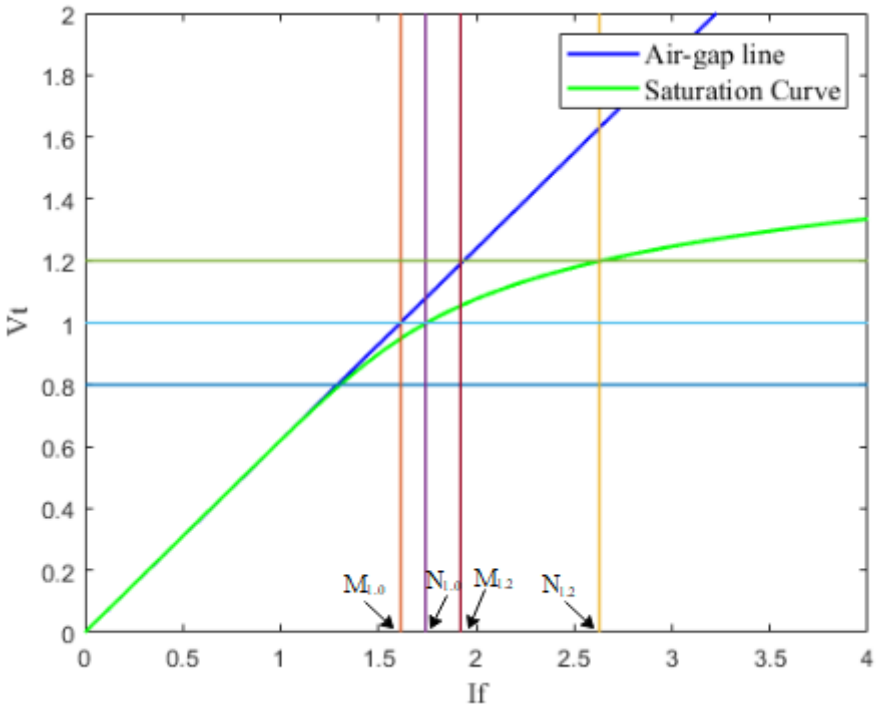

Figure 3-2: Derived OCC of a hydro generator HG1.

In order to calculate the saturation factor four points are marked at the field current axis for rated and 20% overvoltage in both air gap line and saturation curve. These constants are $M_{1.0}$, $M_{1.2}$, $N_{1.0}$ and $N_{1.2}$. The constant M determines the field current on the air-gap line while constant N determines the field current in the saturation curve. Now, the saturation factors $S_{1.0}$ and $S_{1.2}$ are calculated as:

$$S_{1.0}=\frac{N_{1.0}-M_{1.0}}{M_{1.0}} \qquad \text{Equation 3.5}$$

$$S_{1.2}=\frac{N_{1.2}-M_{1.2}}{M_{1.2}} \qquad \text{Equation 3.6}$$

Two saturation constants are calculated using abovementioned saturation factors. Equation 3.7 and Equation 3.8 reveal the equation for calculating saturation factors A_{satu} and B_{satu}.

$$A_{satu}=\frac{S_{1.0}^2}{1.2*S_{1.2}} \quad \text{Equation 3.7}$$

$$B_{satu}=5*\ln\left(1.2*\frac{S_{1.2}^2}{S_{1.0}}\right) \quad \text{Equation 3.8}$$

An exponential function is used to express the saturation factor for all operations. Equation 3.9 provides the saturation factor S. In this case to determine the saturation factor threshold voltage 0.468 is considered.

$$S=A_{satu}*e^{B_{satu}*(E_g-0.468)} \quad \text{Equation 3.9}$$

After that, the saturation factor is transformed into the Ksdm saturation factor. This is carried out because, depending on the saturation level, the armature reaction reactance Xadu can be multiplied by the saturation factor Ksdm to yield a lower value.

$$K_{sdm}=\frac{1}{(1+S)} \quad \text{Equation 3.10}$$

$$X_{adsatu}=X_{adu}*K_{sdm} \quad \text{Equation 3.11}$$

$$X_{dsatu}=X_{adsatu}+X_p \quad \text{Equation 3.12}$$

The use of potier reactance which is higher than the leakage inductance is to calculate saturated reactance to account for the difference between the saturation during the loaded condition and no-load condition, assuming that all load circumstances are steady-state. Now, the following Equation 3.13 and Equation 3.14 can be used to express the field current.

$$E_{gsatu}=Ua*\cos(\delta)+R_a*I_{ar}*\cos(\delta)+X_{dsatu}*I_{ar}*\sin(\emptyset+\delta) \quad \text{Equation 3.13}$$

$$I_{fid}=\frac{E_{gsatu}}{X_{adsatu}} \quad \text{Equation 3.14}$$

3.3 Virtual Visualization of capability curve

All the outlined defining parameters are obtained directly from the process of mathematical calculations to determine the capability chart and the point of operation is continually updated from the PSAT simulation results for this study but in actuality these data can be obtained by measuring units. During operation, active and reactive power, terminal voltage, grid frequency, temperature, and cooling agent pressure are just a few examples of the variables that fluctuate causing the capability diagram to modify its configuration in actual operation time. However, the changes due to temperature and pressure is out of scope of this study. The MW and MVAr coordinate axes remain unchanged, as do other curves such as prime mover power limits. All of the previously discussed factors are incorporated in the MATLAB software [18] environment to produce a comprehensive visual depiction of the capability diagram.

3.3.1 Implementation of capability curve

The capability diagram for the generator is constructed in the MATLAB software environment with the various constraints mentioned in the section 2.5. MATLAB code is used to implement the capability diagram using the visualization tool. This software environment offers an extensive visualization for the capability diagram's implemented mathematical model. The simplification is made by assuming Xd=constant is assumed for the cylindrical rotor machine while the magnetic saturation is calculated and capability curve is redrawn considering the saturation effect for salient pole machines. Based on the abovementioned operating restrictions the procedure for obtaining a cylindrical rotor's and non-cylindrical rotor synchronous generator capability diagram is displayed in this work. The technique relies on the real-time calculation of the generator's capability chart, which takes into account load ability thresholds imposed by generator components. The method for determining the capability diagram's boundary is the emphasized in this subsection. The primary concept and mechanisms involved for the limits are also determined in this subsection. The appendix contains the MATLAB code used to create the capability diagram.

3.3.1.1 Limitation on turbine power:

The maximum power that the generator can produce depends on the capacity of the prime mover [18]. Depending on the relationship between the prime mover's power and the generator's rated power, there will be two criteria for this maximum power limitation. If the prime mover's power is more than the generator's power, then Pmax=Pg and If the prime mover's power is greater than or equal to the generator's rated power (Pt > Pg), then Pmax = Pt.ηg. The Pmax equals to Pg is taken in this case.

The limitation of the minimum power depends on requirements of the turbine. This restriction does not apply to Pelton turbines, although Kaplan, Francis, and other turbine types minimum outputs are restricted to 5% to 30% of the rated output which is not included in this thesis work.

3.3.1.2 Limitation on stator current:

The armature current flowing in the stator is governed by the Iar^2R power loss associated with the stator winding. The synchronous generator MVA rating is limited so that the maximum armature current is carried by the armature winding without exceeding the prescribed heating limits of the machine. The maximum current for the given terminal voltage in the armature can be defined as:

$$S_{max}^2=P^2+Q^2=(V_{tr}I_{armax})^2 \qquad \text{Equation 3.15}$$

The circle-shaped maximum armature current limit is depicted as a circle with center at (0,0) and the radius equals to MVA rating in the two-dimensional plane.

3.3.1.3 Limitation on field current:

In the synchronous generator excitation current is flowing in the rotor winding and is limited by I_{fi}^2R power loss. The generator's excitation system regulates the reactive power. This is due to a field current constraint in the excitation system. E_{01} which is proportional to the generator field current I_{fi}, determines the generation of reactive power for required P and rotor angle δ. The maximal reactive power generated is thus

limited by the I_{fimax}. From Equation 2.7, Equation 2.8 and $\sin\delta^2+\cos\delta^2=1$ the relation for round rotor machine is obtained as:

$$E01=\sqrt{(V_{tr}+I_{ar}Xd\sin\emptyset)^2+(I_{ar}Xd\cos\emptyset)^2} \qquad \text{Equation 3.16}$$

where $cos\,\emptyset$ =P/S. The rotor heating limit is limited by Equation 3.17.

$$P^2+\left(Q+\frac{V_{tr}}{Xd}\right)^2=\left(\frac{E_{01}V_{tr}}{Xd}\right)^2 \qquad \text{Equation 3.17}$$

Then, the field current limit can be represented by the circle defined with a center in $(0,-V_{tr}^2/Xd)$ and a radius of $(E_{01max}\ V_{tr}/Xd)$ for E_{01max}, which corresponds to I_{fimax}. This limit is identified as the maximum field current limit and illustrated in the MW-MVAr plane in Figure 3-3.

Similarly, for salient pole machines the maximum and minimum curves in the field current limit illustrate the relationship between active and reactive power in the case of constant excitation voltage, i.e. constant field current. These limits are determined by the pascal curves resulting from these equations.

$$P=\frac{E_{01}V_{tr}}{X_d}\sin(\delta)+\frac{V_{tr}^2}{2}\left(\frac{X_d-X_q}{X_d*X_q}\right)\sin(2\delta) \qquad \text{Equation 3.18}$$

$$Q=\frac{E_{01}V_{tr}}{X_d}\cos(\delta)-\frac{V_{tr}^2}{X_d}+V_{tr}^2\left(\frac{X_d-X_q}{X_d*X_q}\right)\sin^2(\delta) \qquad \text{Equation 3.19}$$

$$E01=V_{tr}\cos(\delta)+X_d*I_{ar}\sin(\emptyset+\delta) \qquad \text{Equation 3.20}$$

A smallest semicircle of the pascal curve can be plotted with centre at $\left(-\frac{V_{tr}^2}{X_d}*\frac{X_d+X_q}{X_d*X_q},0\right)$ with radius of $\left(\frac{V_{tr}^2}{X_d}*\frac{X_d-X_q}{X_d*X_q}\right)$.Then the point A and B in capability curve can be obtained as:

$$A_x=\left(-\frac{V_{tr}^2}{X_q},0\right) \qquad \text{Equation 3.21}$$

$$B_x = \left(-\frac{V_{tr}^2}{X_d}, 0 \right)$$ Equation 3.22

For the minimum and maximum voltages, the points are marked at $\left(\frac{E_{01min} V_n}{X_d}\right)$ and $\left(\frac{E_{01max} V_n}{X_d}\right)$ in the line drawn from 0 to δ_n starting at point A_x. Because of the unique characteristics of the excitation system, the generator's excitation generally cannot be lower than a particular value. The minimal induced voltage that is permitted was obtained using Equation 3.23, where the k-factor is k=0-0.3 [18], and this is also a Pascal curve.

$$E_{01min}=k*E_{01max}$$ Equation 3.23

3.3.1.4 Limitation on practical stability:

The practical stability limit denotes the highest power angle the generator can run at without losing grid synchronization. The electromagnetic torque and mechanical torque are no longer balanced when the power angle is raised over the breakover angle. It is possible to determine the breakover angle at which Pmax is reached. The natural stability limit is expressed by Equation 3.24 and Equation 3.25, to calculate the maximum load angle as a parametric curve.

$$\frac{dp}{d\delta}=0$$ Equation 3.24

$$\cos(\delta)=0.25*\left(-\frac{E_{01}X_d}{V_{tr}(X_d-X_q)} + \sqrt{\left(\frac{E_{01}X_d}{V_{tr}(X_d-X_q)}\right)^2 +8} \right)$$ Equation 3.25

But owing to the ease by which slipping out of synchronism could be caused by a minor load increase, this limit does not offer safe operating conditions for generator operation. Thus, to maintain a practical stability margin, taking 10% of the machine's rating as a safety boundary the theoretical stability curve can be reduced to 0.1*RatedMVA of a machine. The realistic stability limit can be represented as the curve starting at a smaller pascal curve and gradually increasing.

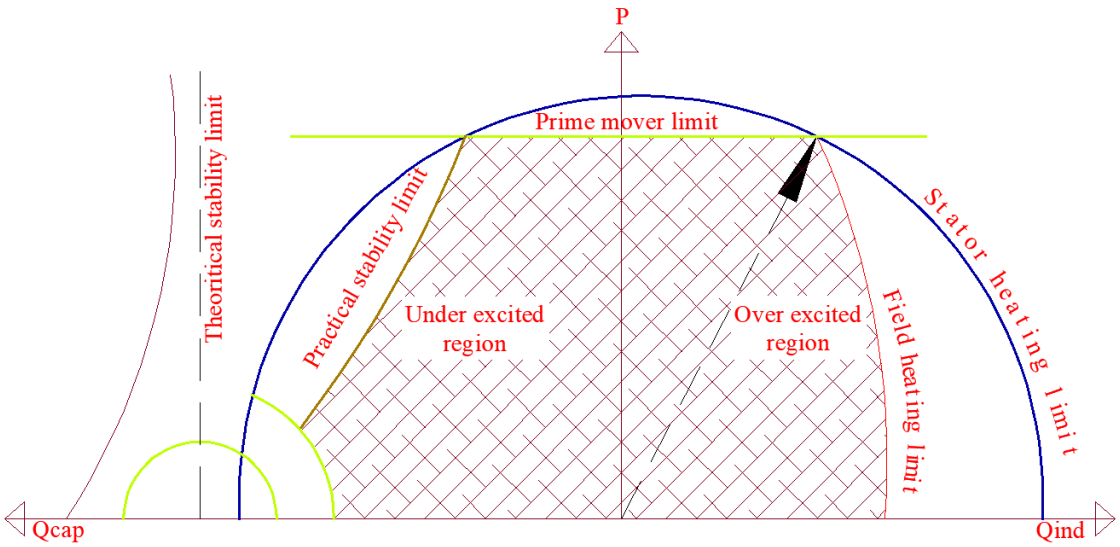

Figure 3-3: Limits on the generator capability curve.

The safe operating zone for the generator is inside the boundary of above mentioned limits.

3.4 Time Domain Dynamic Simulation

A time domain simulation is carried out to examine the system's behavior in the presence of perturbations. After causing some disruption in the lines, loads and buses, the voltages at various buses are analysed. Momentary disruptions are applied at various locations across the system's and response is studied. The computation of the power flow analyses data using the Newton Raphson Method and in time domain simulation, trapezoidal integration is employed. To complete the aforementioned two tasks, MATLAB's Power System Analysis Toolbox [19] is used. The output generated after time domain simulation are utilized for the operating points on the capability curve.

CHAPTER 4:SYSTEM MODELING AND SIMULATION

In this study the Power System Analysis Toolbox (PSAT) is utilized for the simulation setup for the test systems that has been used for disturbance scenario analysis in voltage fluctuations and the MATLAB platform is used for the visualization of the synchronous generator's capacity curve.

4.1 Case study of hydro generator

In order to estimate the saturation in the synchronous machine and to visualize the capability curve of the salient pole synchronous generator, one hydro generator (HG1) from Brazil's Furnas hydroelectric project, which was referenced in Bortoni's technical report [3], is taken into consideration in this analysis. The rated parameters of that generator are presented in Table 4-1 To show the basic mechanisms restricting the capability diagram, the quantities limiting the generator are obtained as described in section 2.5. To demonstrate the critical parameters limiting generator HG1 capability diagram, the boundaries are drawn in MATLAB.

Table 4-1: Rated parameters of Hydro generator HG1.

Description	Symbol	Value
Apparent power	S	160 MVA
Power factor	cos ∅	0.95
Rated armature voltage	Vt	15 kV
Rated armature current	Ia	6185 A
Rated field current	If	1047 A
Rated frequency	F	50 Hz
Armature resistance	Ra	0.00232 pu
Direct-axis reactance	Xd	0.8 pu
Quadrature-axis reactance	Xq	0.6 pu
Potier reactance	Xp	0.18 pu
Rated efficiency	ηl	98.5%

4.2 Power System Analysis Toolbox (PSAT)

PSAT is a MATLAB-based toolkit for electric power system analysis and control. Power flow, continuous power flow, optimal power flow, tiny signal stability analysis, and time domain simulation are among the subjects studied. It has graphical user interfaces (GUIs) for all of its functionalities, and a Simulink-based library for quick access to network design tools.

4.2.1 Time Domain Analysis in PSAT

The time domain simulation was run for the whole 20 seconds, and the results showed that the system was stable. It can be shown that the voltage becomes unstable following the application of faults. The findings for the fluctuations in the bus voltage are compared with three different scenarios of contingencies in this work. The entire bus system was disrupted after the occurrence of the events.

4.3 Test system's overview

The simulations are based on available bus, generator and line data as used in IEEE 9 bus test system (test system 1 now onwards) with qualitative comparison in IEEE 14 bus test system (test system 2 now onwards) connected to an infinite bus bar. The modeling and simulation was carried out using the MATLAB and Power System Analysis Toolbox (PSAT) program [19].

Actually, the test systems employed for the study is based on the system specified in [20] and [21]. Figure 4-1 and Figure 4-2 displays the comparable single line diagram of the IEEE 9-bus and IEEE 14-bus test network. In Figure 4-1, the units G1, G2, and G3 are synchronous generators (SG) that are computationally represented as emf (E01) behind the synchronous reactance. The reactance of the three step-up transformers (T1, T2, and T3) are used to represent them. The step-up transformer connects each generator to the bus. The plant's 230kV bus bars are connected to each of the three generators (G1, G2, and G3). IEEE 9 bus test power system is used to obtain the operating parameters and implement the capability curve for generator G3. The power system consists of 9 buses, 6 lines, 3 tap changing transformers placed replacing normal transformers, 3 generators on buses 1, 2 and 3 and loads on buses 5,6 and 8.

In Figure 4-2, the units G1 and G2 are synchronous generators (SG) and C1, C2 and C3 are synchronous condensers. The plant's bus bars are directly connected to each of the two generators (G1, and G2). IEEE 14 bus test power system is used to obtain the operating parameters and implement the capability curve for G2. The standard 14 bus test scenario has five generators, eleven loads, and fourteen buses. The system parameters are modified including few contingencies in both test systems for the study purpose.

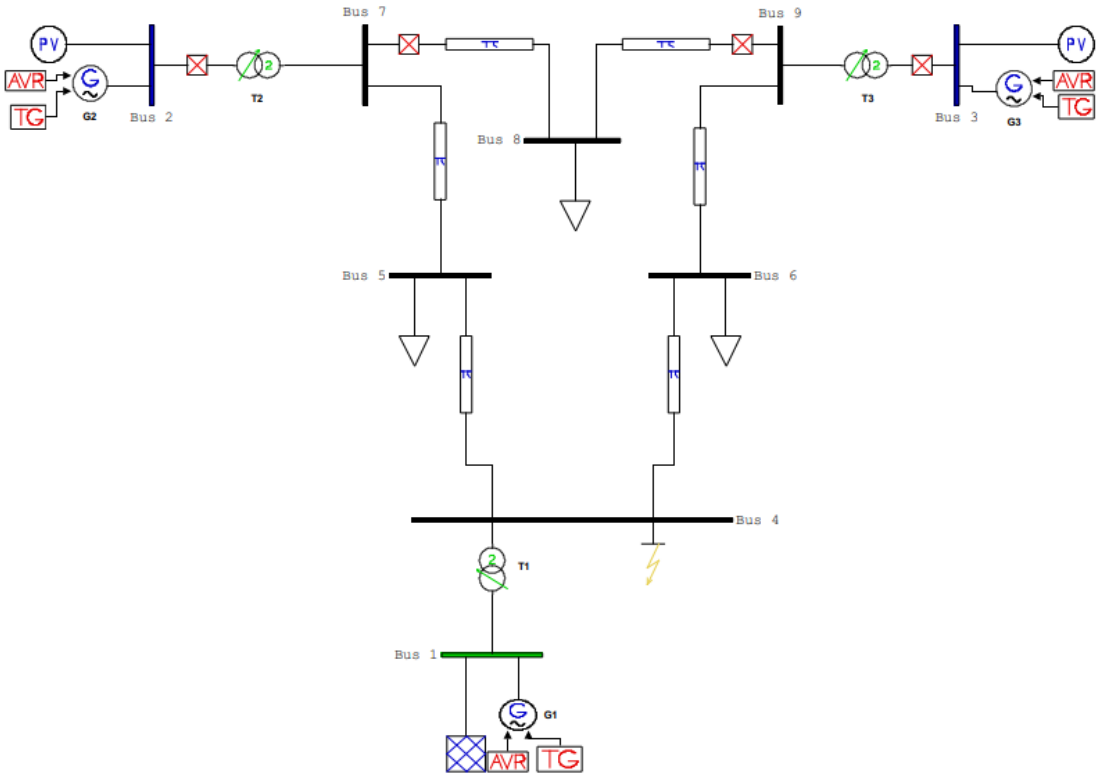

Figure 4-1: Single line diagram of IEEE 9 bus test system in PSAT.

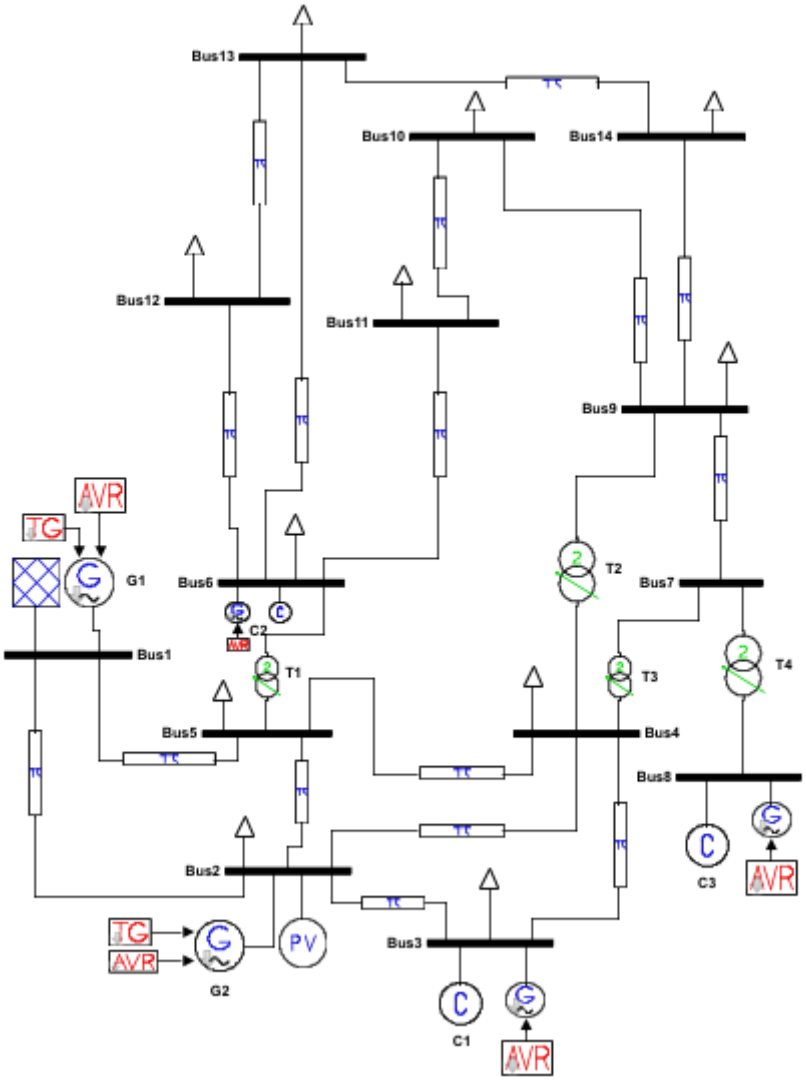

Figure 4-2: Single line diagram of IEEE 14 bus test system in PSAT.

4.4 Contingency Selection

The process of contingency selection is required to assist stable operation of power systems and for planning for transmission expansion [22]. This procedure focuses on finding the situations that result in the operational boundaries being violated. Power System Analysis Toolbox (PSAT) is used to simulate the test system's simulation setup for the voltage variation study, and the MATLAB platform is utilized to visualize the generator's capability curve and operating points variation. This study investigates how the contingencies in the power system network impacts on the operation of the generator and bus voltage post-disturbance.

4.4.1 Normal Operation

The steady state operation of the test system with voltage profiles at different buses is shown in Figure 4-3 and Figure 4-4. During the normal operation voltage at all of these buses is within the limits.

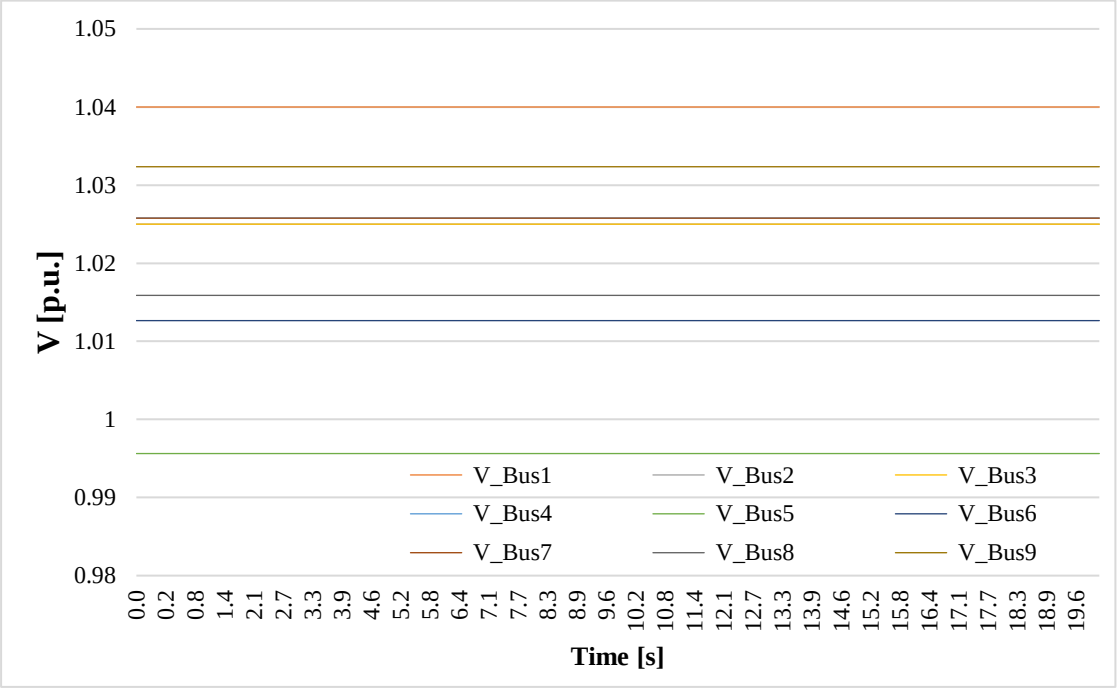

Figure 4-3: Bus voltages at normal operating condition for test system 1.

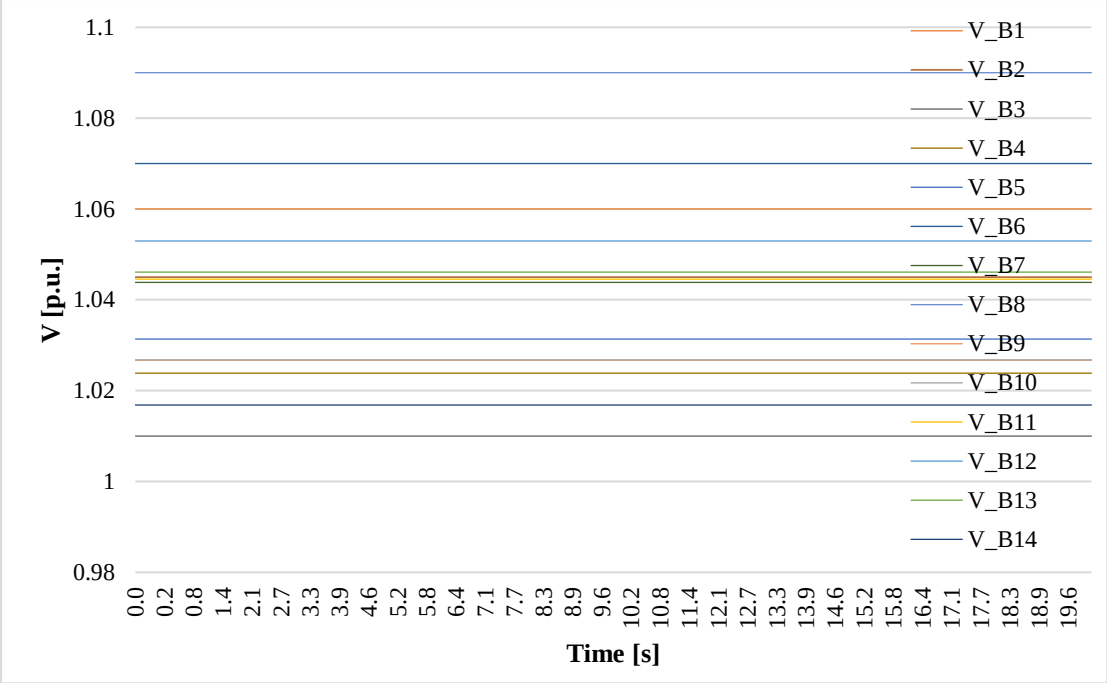

Figure 4-4: Bus voltages at normal operating condition for test system 2.

4.4.2 Scenario 1: Line Outage

In order to analyze the change in the operating range of the connected generators and buses the loss of one line 8-9 of test system 1 and line 4-5 of test system 2 at 0.25 sec and restored after 1.5 sec is simulated in PSAT and it is found that the voltage at the nearby buses from disrupted buses are disturbed more and after the removal of the outage gradually moved towards stabilization maintaining voltage stability.

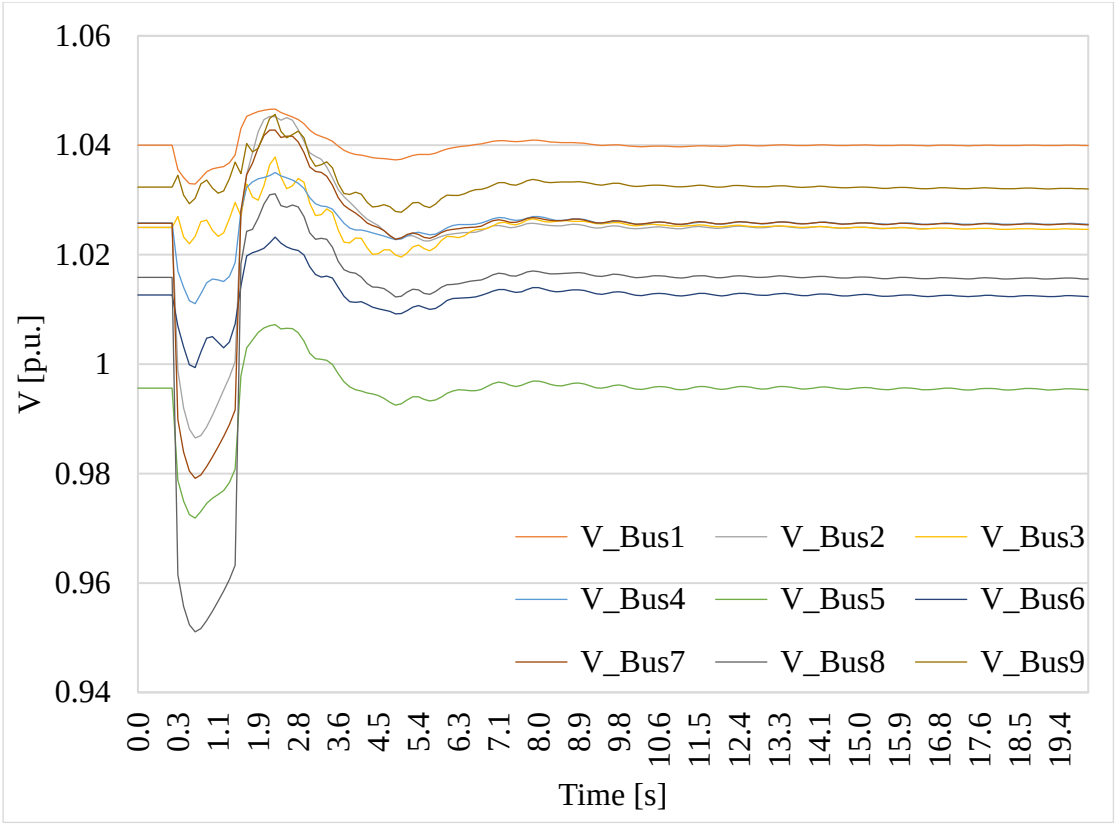

Figure 4-5: Bus voltages during the outage of line 8-9 of test system 1.

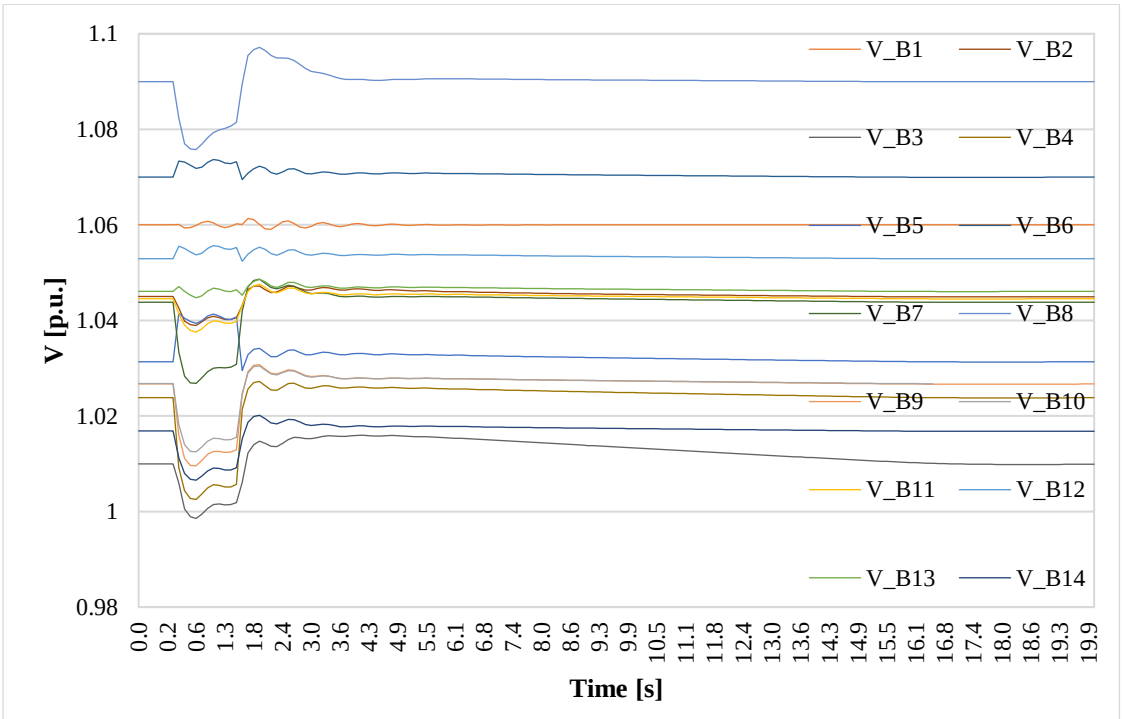

Figure 4-6: Bus voltages during the outage of line 4-5 of test system 2.

4.4.3 Scenario 2: Load Outage along with Line Outage

An analysis of the test system is done considering the outage of line 7-8 for test system 1 and line 2-4 of test system 2 at 1.25 sec with restoration at 5 sec and the reduction of load at bus 8 and bus 4 to zero for first system and second system respectively.

After time domain simulation it is observed that due to the removal of load at bus 8 only after the outage of line 7-8 voltage at buses kept fluctuating and the transient is minimized after the removal of the line disturbance. The voltage at all buses is still within the stability region.

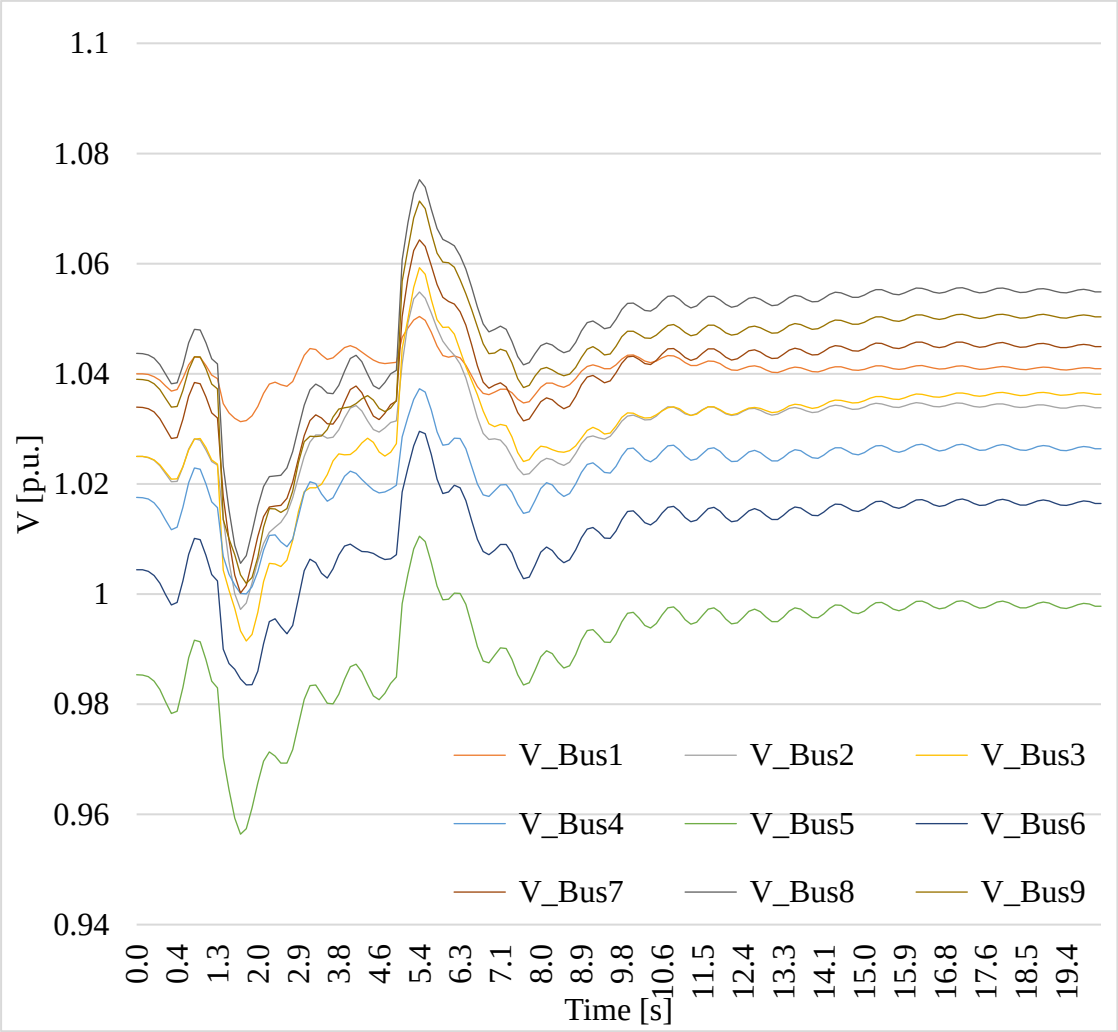

Figure 4-7: Bus voltages during the outage of load at bus 8 and loss of line 7-8 of system 1.

Similarly, in case of load outage in bus 4 of test system 2 slight increment in voltage is observed initially but only after line 2-4 outage voltage started fluctuating and remained stable after the removal of disturbance.

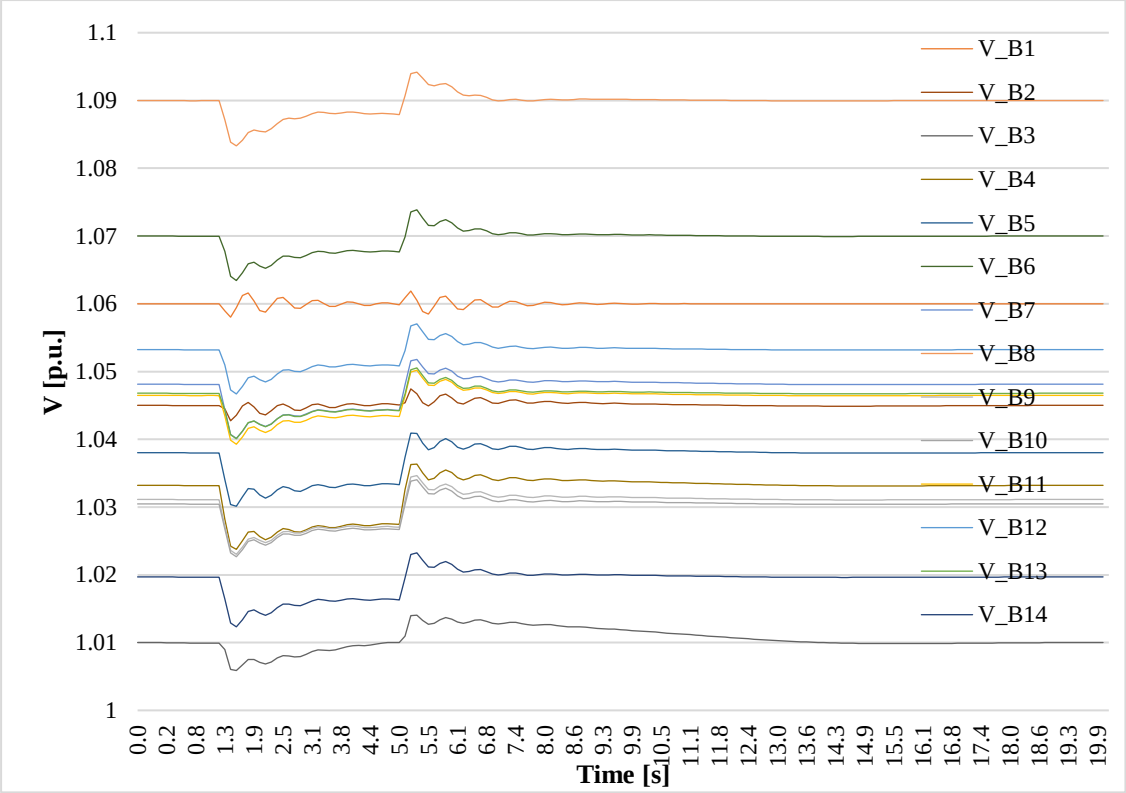

Figure 4-8: Bus voltages during the outage of load at bus 4 and loss of line 2-4 of system 2.

4.4.4 Scenario 3: Three Phase Fault at Bus

In this study, a three-phase fault at busbar 4 of test system 1 and busbar 6 of test system 2 is taken into account when performing disturbance scenario analysis. The three-phase fault is created in both bus bars at time 0.7 sec and is cleared after time 1 sec. The results show that the voltage at all buses fluctuated during fault conditions and it reached the condition of voltage instability in case of system 1 but in case of system 2 all buses reached the condition of voltage instability except bus 1,2,3 and 8 being far from the disturbance. At the fault clearing times of 1 second, the all busbar voltage collapses for the first system while only four of the buses of second system are within limit.

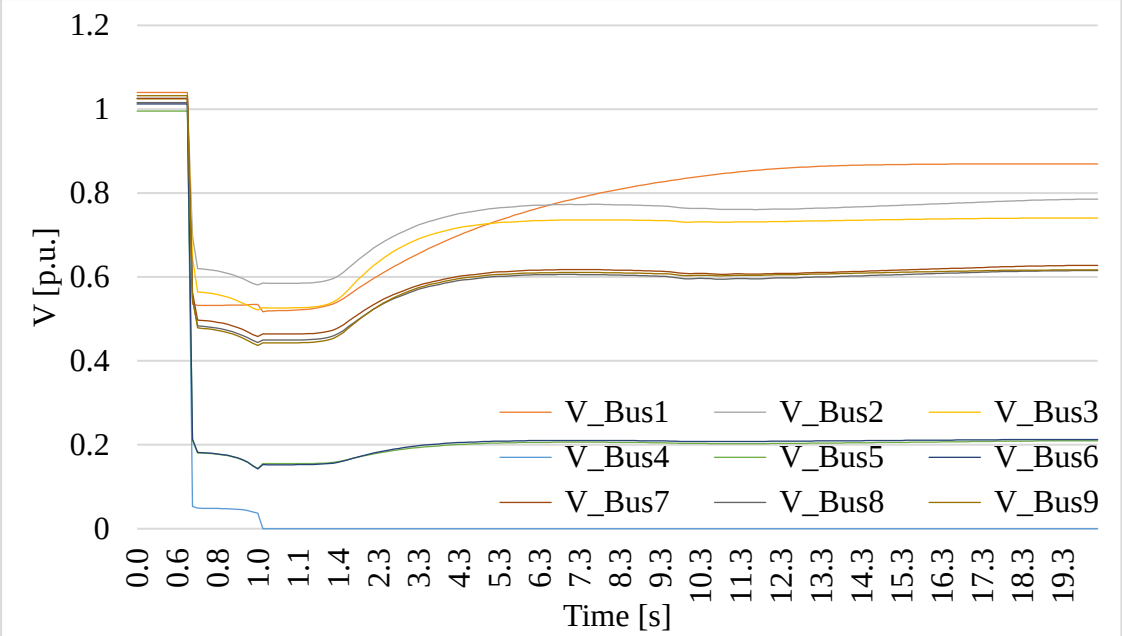

Figure 4-9: Bus voltages during the three-phase fault at bus4 of test system 1.

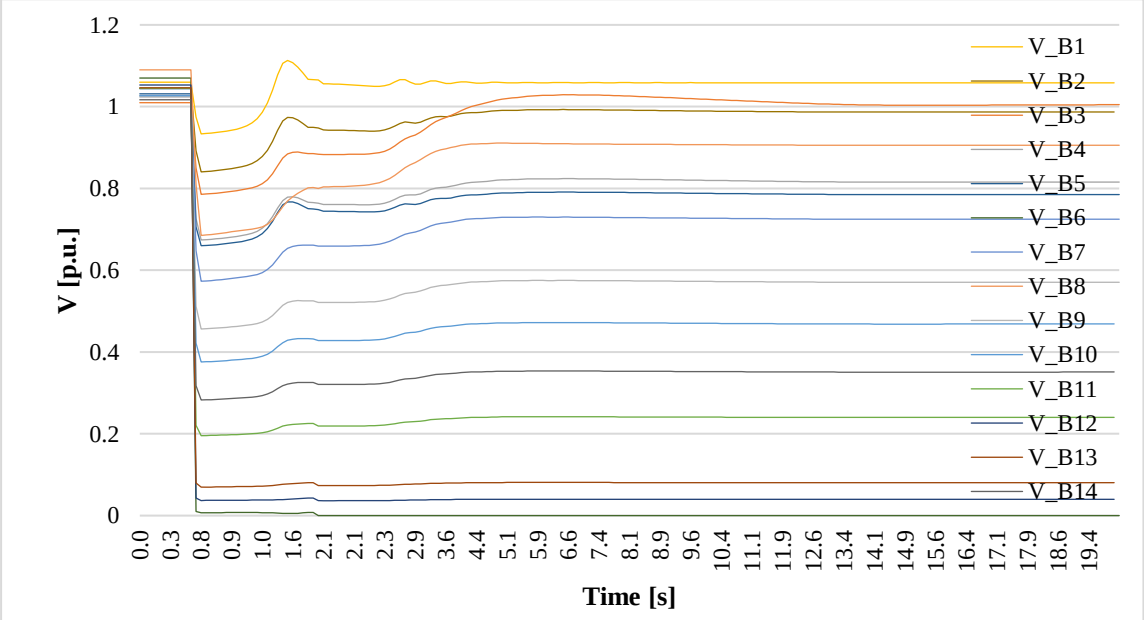

Figure 4-10: Bus voltages during the three-phase fault at bus6 of test system 2.

From the comparative analysis of bus voltages for common types of disturbances in two of the test systems it can be observed that the disturbance is more severe in first test system i.e. the transients settle down slowly in the first test system as compared to second one it can be due the increment in the second system's size.

4.5 Automatic Capability Curve Visualization Tool

Implementation of different operational limits in capability diagrams using the MATLAB software environment was described in section 2.5. MATLAB App designer was used to construct a visual App for better diagram visualization of the operating condition of the round rotor synchronous machine. The case study of the IEEE 9-bus test case and IEEE 14-bus test case described in section 4.3 served as the foundation for all parameter values that were implemented and the dynamics that were seen in the visualization tool. A simple workflow diagram utilized during the incorporation of the capability diagram for the generator in the visualization tool is displayed in Figure 4-11. Two figure windows and three tabs make up the GUI. The capability chart with the simulated operating point is displayed in the upper figure window (1) of the user interface and is denoted by a "red" asterisk symbol. The active and reactive power variation is displayed in the window (2). The parameters tab (3) and (5) shows the rated generators data and operational data at the end of simulation. The tab (6) is for the P and Q limit in per unit.

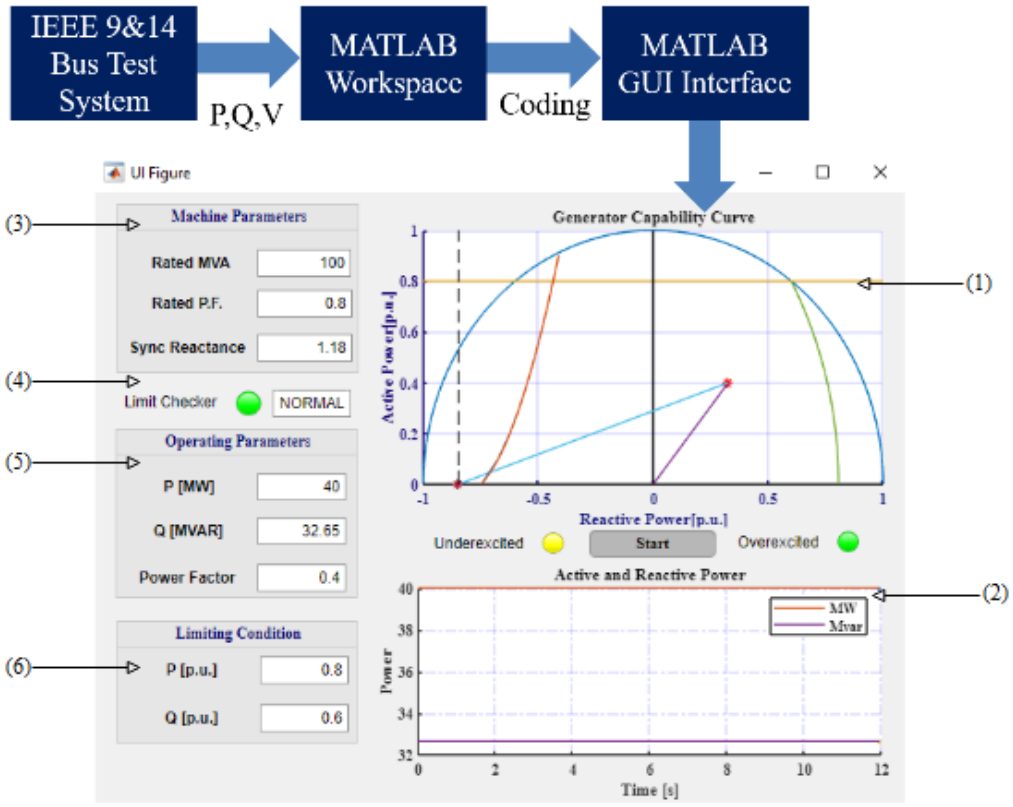

Figure 4-11: Workflow schematic for visualization of generator capability diagram.

The limits are indicated by the three yellow lamps, limit checker lamp glows green during normal operation with ‘NORMAL’ indication and changes to red after violation of operational limits displaying ‘ALARM’. The Operating conditions lamps show either the generator is operating on under excitation or overexcitation by a lamp glowing green.

CHAPTER 5:RESULTS AND DISCUSSIONS

In order to develop a capability diagram of any generators and to determine the operation of any connected generator of a power system, this study set out to create a software in MATLAB. This software tool is utilized in this study to observe the operating points of generators in case of emergency in the network. This ensures greater exploitation of the synchronous generator by providing better insight into the operational constraints.

5.1 Saturation calculation validation

In the case study described in the preceding section, the field current is calculated analytically using the methods presented in section 3.2. The calculated results are contrasted with the field current from an industrial hydro-generator being studied (HG1) as mentioned in rated value. Utilizing the field current measurements taken at one maximum loading point, the techniques are experimentally confirmed.

The open-circuit characteristic (OCC) of the generator is used for calculation in this study. The Anderson and Fouad approach is used to consider saturation in this research work. Here, the generator hits a threshold voltage of Eg = 0.63 pu, when the saturation increment occurs. In order to quantitatively verify the calculated quantities are compared with the measured quantities at a maximum loading point as shown in Table 5-1.

Table 5-1: Saturation validation for HG1.

Description	Value
Measured If	1047 A
Calculated If	1248.70 A

5.2 Capability curve of salient-pole machine

To visualize the capability curve of a salient pole machine only a static capability diagram is plotted marking the operational boundary. While, the complete visualization tool is utilized for the operating points variation study in case of round rotor machines

of the test system in later sections. Based on the technique discussed in section 2.5 for construction of the capability diagram of the non-cylindrical rotor machine, the capability diagram is obtained for the rated d-axis reactance and saturated d-axis reactance. As previously discussed, saturation of q-axis reactance is not mentioned in this research work.

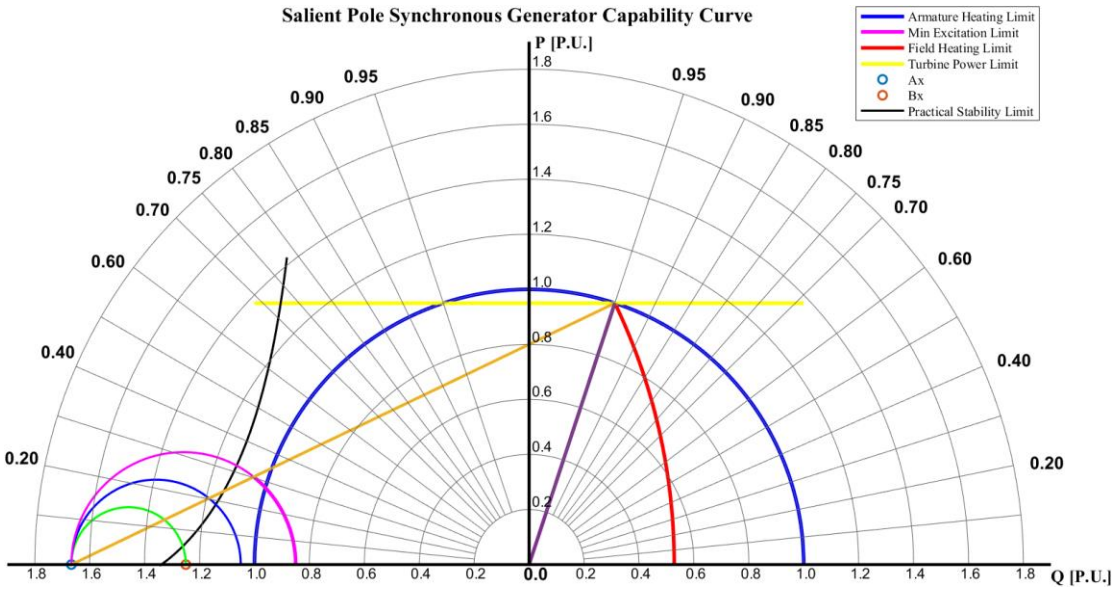

Figure 5-1: Salient pole synchronous generator capability chart.

The stator current restrictions, or perceived power limitation, are shown by the blue circle. The red arc represents the generator's highest induced voltage (Emax). The generator's minimal permitted induced voltage (Emin) is represented by the magenta arc. Also, the prime mover limit is shown by the yellow line. Figure 5-1 displays all the crucial traits of generator HG1 at unsaturated d-axis reactance. The rating data, which are significant parameters restricting the capability diagram, are shown in Table 4-1. In a similar way the capability curve is developed using saturated reactance of Xd_sat=0.7252 as depicted in Figure 5-2.

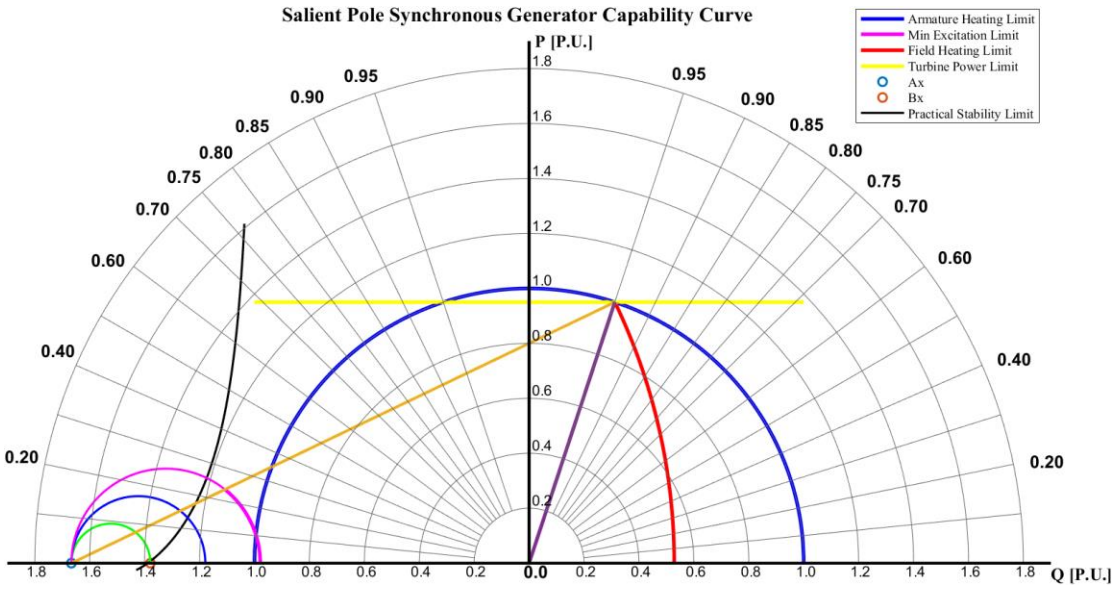

Figure 5-2: Salient pole synchronous generator capability chart for saturated Xd.

5.3 Capability Diagram Visualization Tool

An automatic tool for the scenario-based capability curve visualization was developed using the MATLAB App designer [23]. By applying the operating constraints through MATLAB code, a graphical user interface (GUI) is developed to monitor the operating points of the generator of the round rotor synchronous machine. The GUI consists of an input taking and output generating function, in which based on the input variables the capability curve is plotted and the limits are checked in a similar manner. All the operating points in this tool are based on the case study of the test system 1 and 2, which is discussed in the preceding section. This test system served as the foundation for all parameter values that are implemented and the dynamics that is seen in the visualization tool.

This thesis work demonstrates how to construct a synchronous generator capability diagram assisting the cylindrical rotor capability curve using the following simplifications:

- Taking direct-axis synchronous reactance constant, neglecting machine saturation.
- The impact of armature resistance is neglected.

- The synchronous generator has been considered to be connected to an infinite bus.

The capability diagram is determined using the following rated characteristics for generator G3 in the IEEE 9-bus system and generator G2 in the IEEE 14-bus system:

Table 5-2: Rated parameters of generator G3 of test system 1.

Rated terminal voltage	13.8 kV
Rated MVA	128 MVA
Rated power factor	0.85
Direct axis synchronous reactance	1.3125 p.u.
Practical stability margin	10%

Table 5-3: Rated parameters of generator G2 of test system 2.

Rated terminal voltage	13.8 kV
Rated MVA	100 MVA
Rated power factor	0.8
Direct axis synchronous reactance	1.18 p.u.
Practical stability margin	10%

In MATLAB, Graphical User Interface (GUI) based capability diagram visualization tool is implemented to observe the change in operating scenario of the generator in case of events in the connected network. The rated parameters of generator G3 of the first network and G2 of the second network is given in Table 5-2 and Table 5-3.The visualization tool of generator G3 in normal and G2 in disturbance situations is depicted in Figure 5-3and Figure 5-4 respectively.

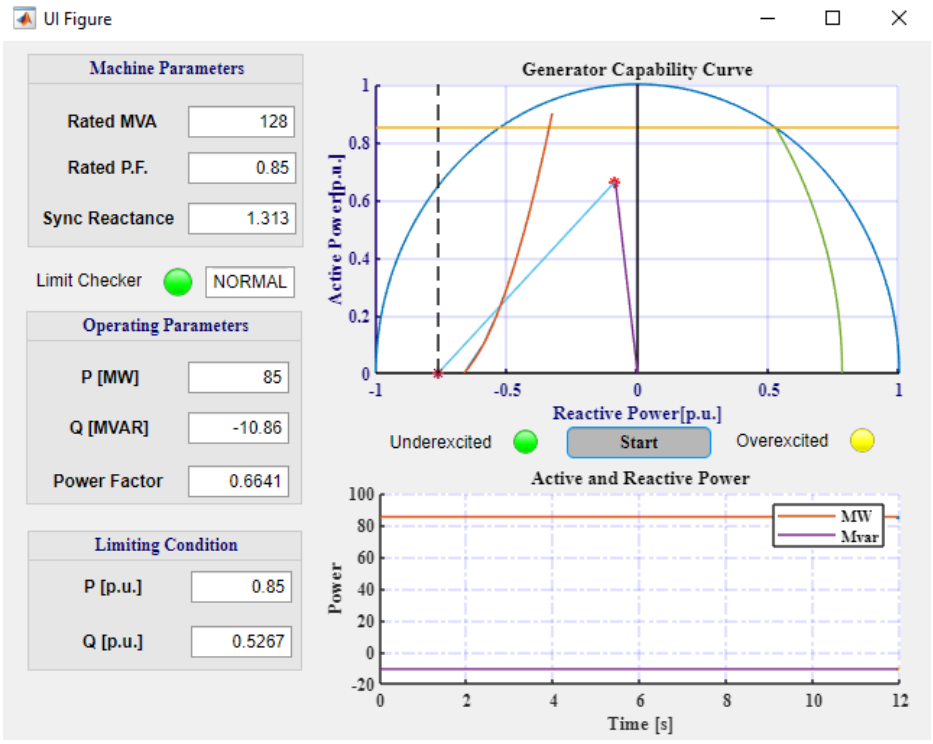

Figure 5-3: Capability curve visualization tool during 'NORMAL' operating condition.

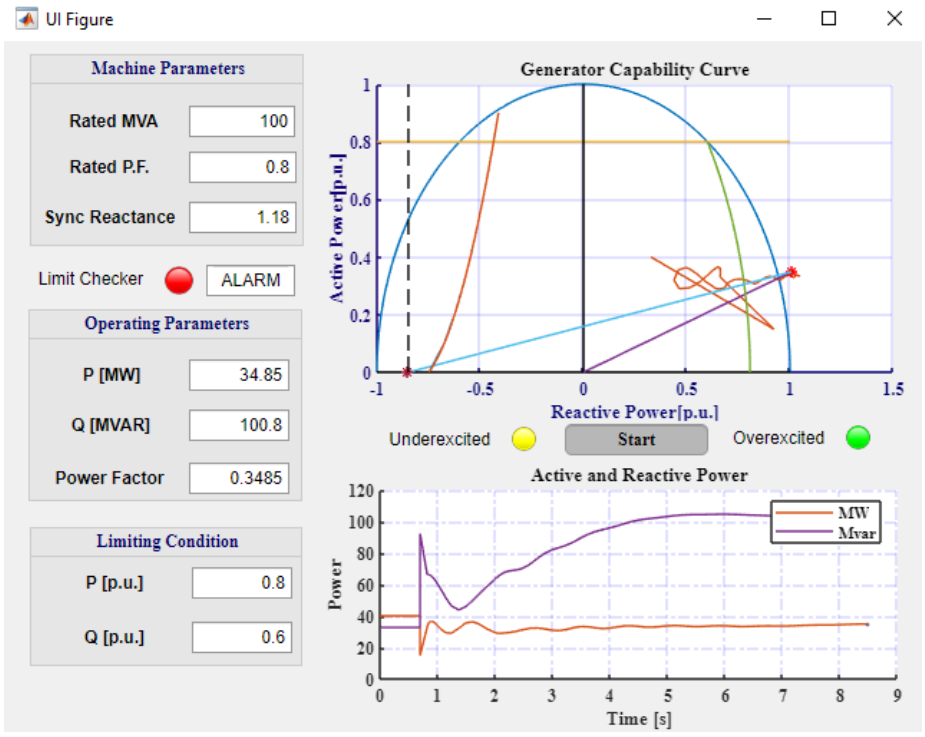

Figure 5-4: Visualization tool at extreme operation displaying 'ALARM'.

5.4 Variation on Capability Curve during Events

This research aims to explore the capability curve operational modification in case of potential contingencies. The operational changes that occurred during the above-mentioned scenarios are revealed in the capability curve. The operating points of generator 3 of the first test system and generator 2 of the second test system can be realized from Figure 5-5 to Figure 5-12.

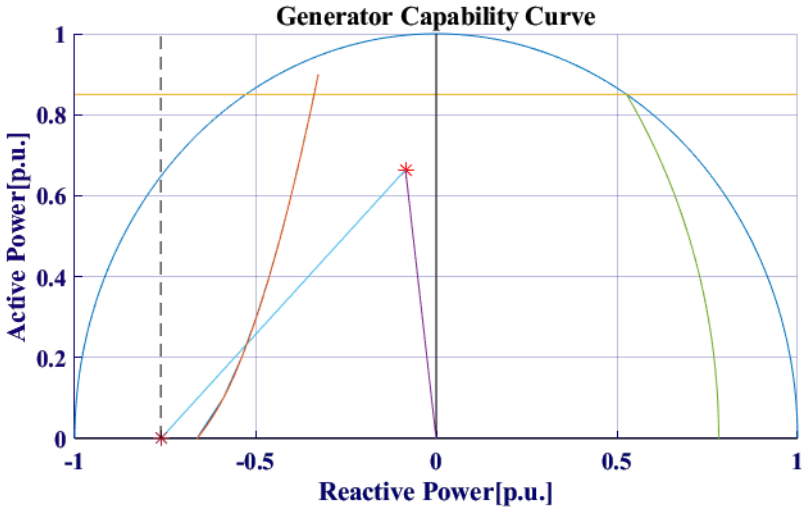

Figure 5-5: Generator 3 operation during normal operation.

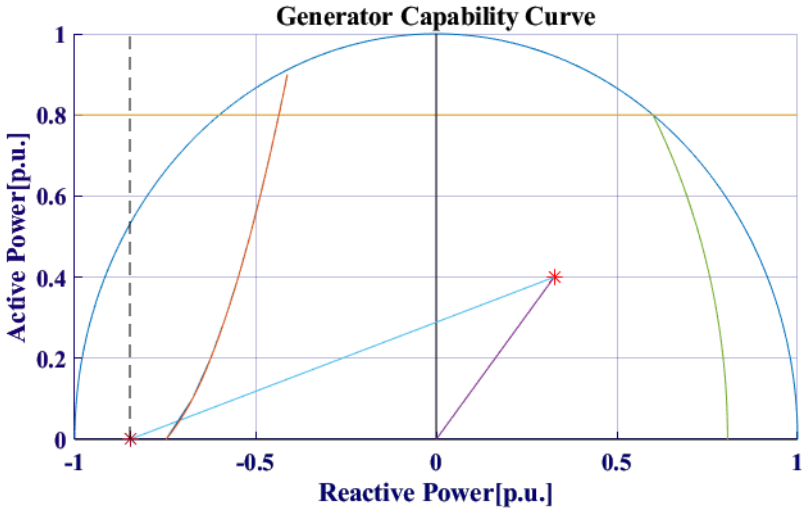

Figure 5-6: Generator 2 operation during normal operation

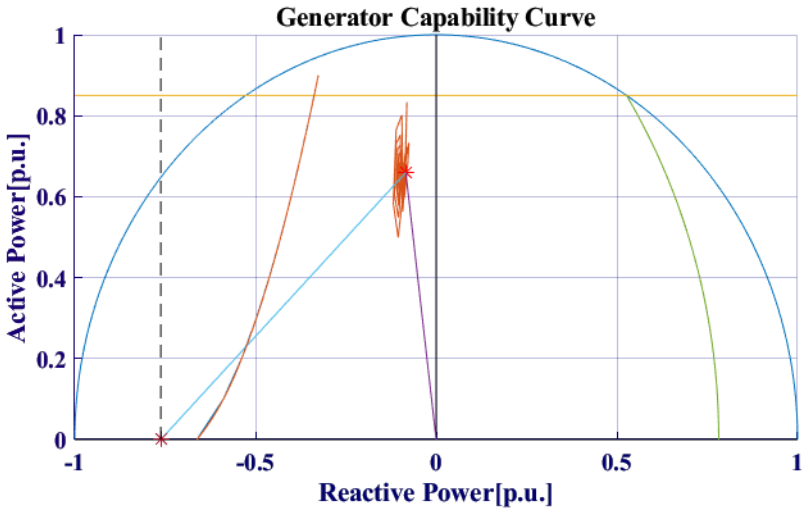

Figure 5-7: Generator 3 operation during line 8-9 outage.

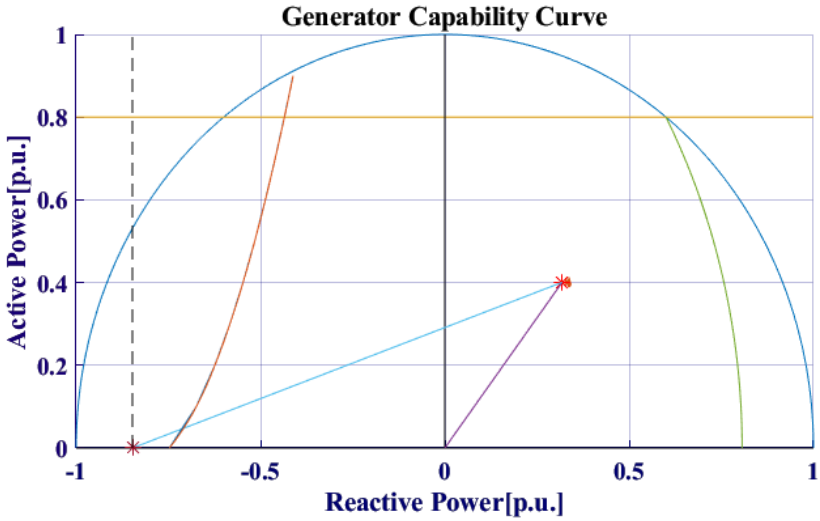

Figure 5-8: Generator 2 operation during line 4-5 outage.

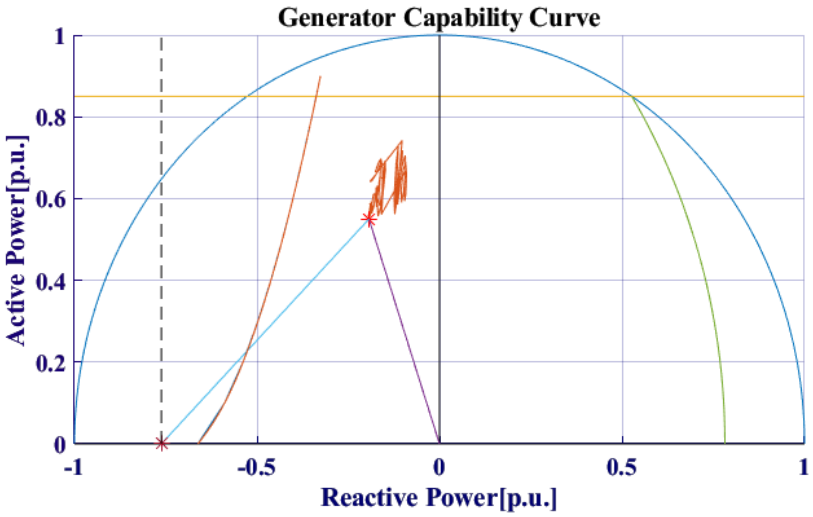

Figure 5-9: Generator 3 operation during line and load outage.

G3 operates at an under excited region during line 8-9 outage, while it is operating with reduced active and reactive power in the event of load outage at bus 8 and line 7-8 loss.

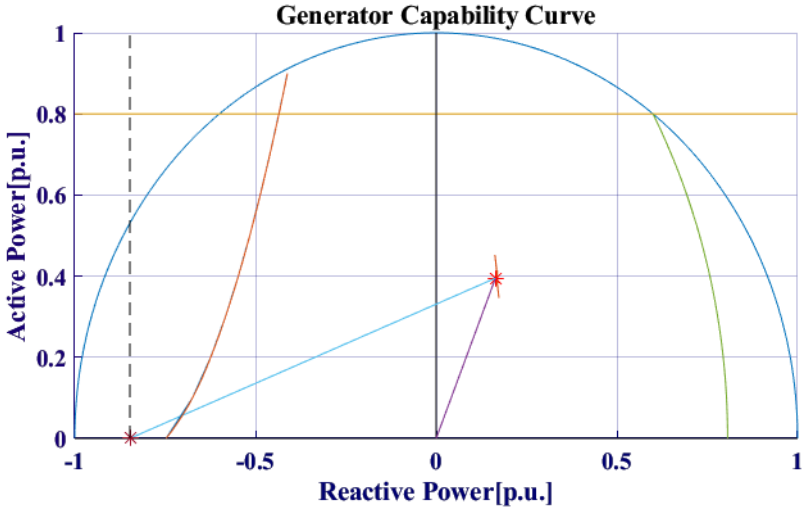

Figure 5-10: Generator 2 operation during load and line outage.

G3 operates at a overexcited region during line 2-4 outage, while it is operating with reduced reactive power in the event of load outage at bus 4 and line 2-4 loss.

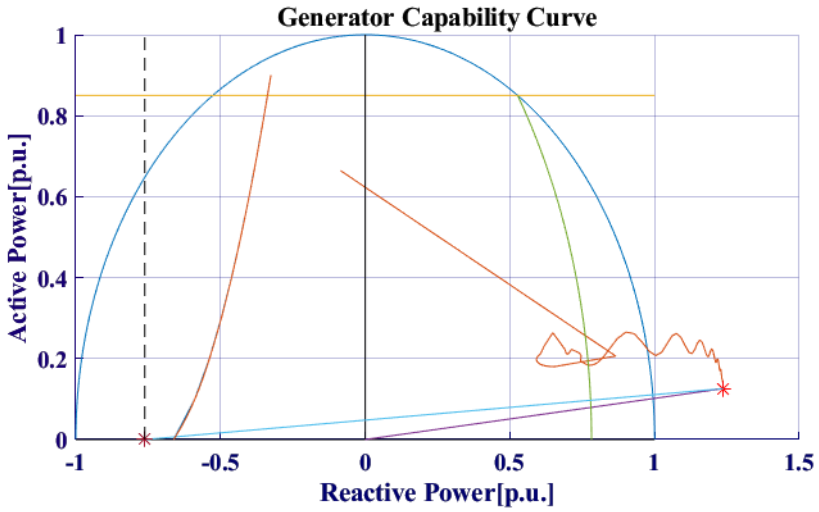

Figure 5-11: Generator 3 operation after three-phase fault.

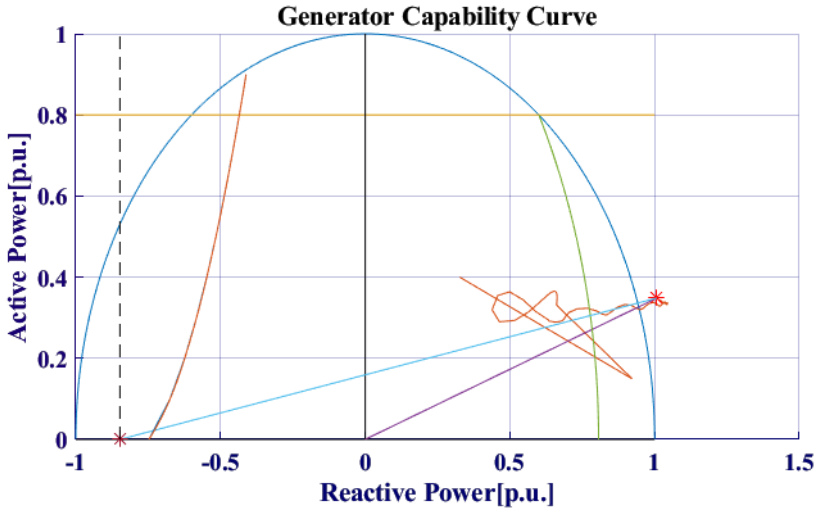

Figure 5-12: Generator 2 operation after three phase fault.

After a three-phase fault in busbars the operation of both generators G3 and G2 reached beyond operational limit following loss of stability.

5.5 Impact of Tap Position on Reactive Power

When synchronized in parallel to the power supply, large synchronous generators can be controlled by using terminal voltage control. Usually, the terminal voltage of these equipment is regulated. In order to investigate the change in the reactive power supply and consumption of connected generators or condenser during the increment or

decrement of the tap position of the tap changing transformer reactive power fluctuation during normal, lower tap at 0.95 pu and higher tap at 1.05 pu is observed.

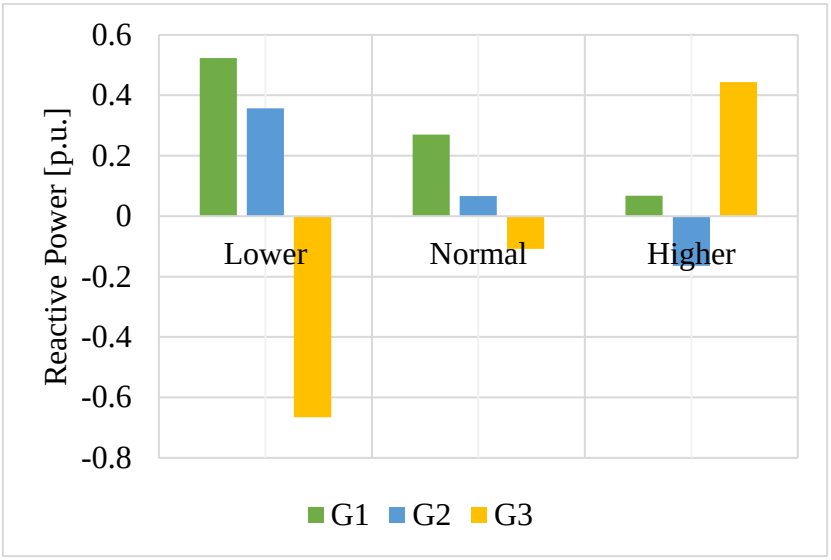

Figure 5-13: Reactive power variation in G1, G2 and G3 of test system 1.

During the lower tap G1, G2 are delivering reactive power and G3 is consuming reactive power and moving to normal and higher tap position the reactive power supplied by G1 is decreased G2 starts consuming at higher tap while G3 starts delivering reactive power at higher tap.

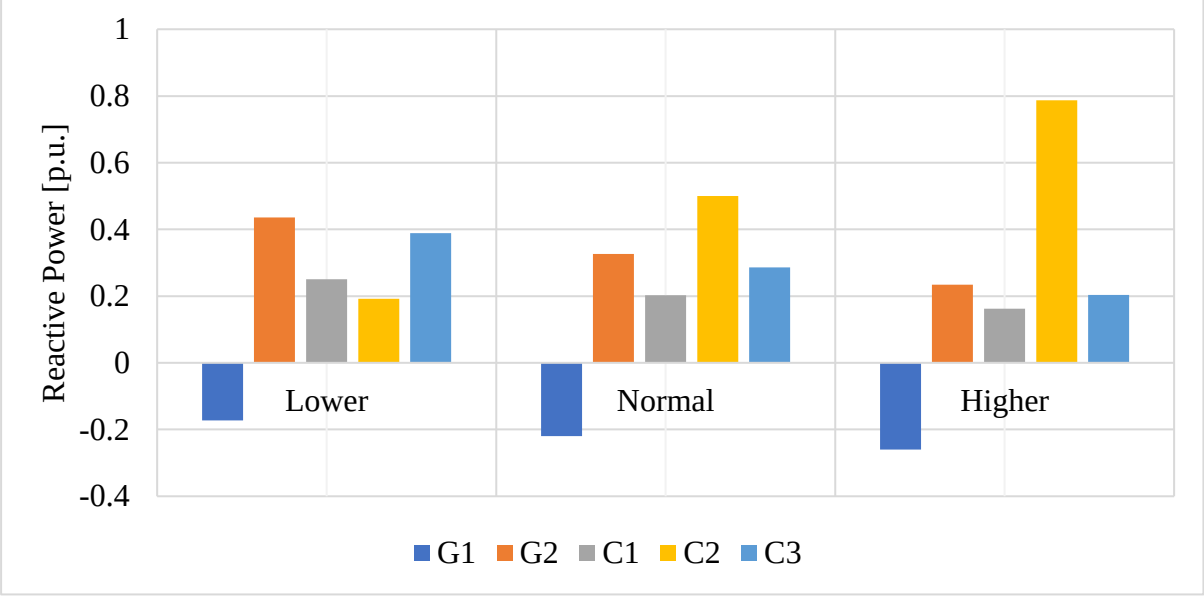

Figure 5-14: Reactive power variation in G1, G2, C1, C2 and C3 of test system 2.

In case of second system as described in section 4.3 only G1 is consuming reactive power in any tap position beside it G2, C1 and C3 has decrement in reactive power supply and C2 has increment in supply of reactive power with the enhancement in tap position of connected transformers.

CHAPTER 6:CONCLUSION AND FUTURE WORKS

This study discussed the methodology for the identification of actual capability diagram to help for the allocation of daily active and reactive power for both cylindrical and non-cylindrical type rotor. The effect of magnetic saturation is analyzed for salient pole synchronous generator while operating condition of an individual generator connected in the network is analyzed for round rotor generators, G3 of test system 1 and G2 of test system 2. The impact analysis in the IEEE 9 and 14 bus test cases depicted that the line disturbance and load variation impacts on the voltage of the buses for fault duration, with the stable operation. However, the three-phase fault on the busbar resulted in voltage instability in the system even after the removal of the disturbance scenario. The work can be used to identify the generator and the bus that will be impacted following a disturbance. By using these findings in the observation of a power system's static and dynamic behavior, the aforementioned analysis presents a very clear picture regarding the defense to secure the power system.

This thesis work has demonstrated the implementation of generators capability curve in MATLAB as a numerical tool for calculations and displaying outcomes and use of PSAT allows full analysis of both static and dynamic situations. The different outcomes that could happen during the actual operation is shown by the simulation. This study could be advanced by atomizing the entire procedure. This implies hat the capability diagram and level of saturation would both be calculated simultaneously by the algorithm using specified inputs. Also, efficiency calculation can be done in detail to obtain the losses in the machine. In light of this, it is advised that future studies focus on obtaining improved capability diagram by comparing the created PQ diagram to one of a real-world unit. The similar scenario analysis can be analyzed in the real power system or other test system to identify post disturbance Impact on voltage instability using any of the other simulation tools.

PUBLICATION

B. Gyawali, N. R. Karki, “Determination of Generator’s Capability Curve and Monitoring Impact of Generating Transformer Tap Changer on Reactive Power Output”, International Conference on Role of Energy for Sustainable Social Development, 8th-9th August 2022, Bhaktapur, Nepal.

REFERENCES

[1] Y. C. Karekezi, T. Øyvang and J. K. Nøland, "The Energy Transition's Impact on the Accumulated Average Efficiency of Large Hydrogenerators," *IEEE Transactions on Energy Conversion,* vol. 37, pp. 2069-2079, 2022.

[2] bp, "bp Statistical Review of World Energy," bp, 2022.

[3] E. d. C. Bortoni, R. T. Siniscalchi, S. Vaschetto, M. A. Darmani and A. Cavagnino, "Efficiency Mapping and Weighted Average Efficiency for Large Hydrogenerators," *IEEE Open Journal of Industry Applications,* vol. 2, pp. 11-20, 2021.

[4] A. Joswig and M. Baca, "Extended requirements on turbo-generators and solutions for flexible load operation," in *2016 XXII International Conference on Electrical Machines (ICEM),* 2016.

[5] I. Ilic, A. Viskovic and M. Vrazic, "User P-Q diagram as a tool in reactive power trade," in *2011 8th International Conference on the European Energy Market (EEM),* 2011.

[6] P. Kundur, Power System Stability and Control, McGraw Hill, 1994.

[7] L. Rouco, K. Chan, J. Oesterheld and S. Keller, "Recent evolution of European grid code requirements and its impact on turbogenerator design," in *2012 IEEE Power and Energy Society General Meeting*, 2012.

[8] M. Kostić , S. Milić and N. Georgijević, "Comprehensive analysis of on-site method for determining synchronous reactance," *International Journal of Electrical Power & Energy Systems,* vol. 121, pp. 106-135, 2020.

[9] F. P. De Mello and L. H. Hannett, "Validation of Synchronous Machine Models and Derivation of Model Parameters from Tests," *IEEE Transactions on Power Apparatus and Systems,* Vols. PAS-100, pp. 662-672, 1981.

[10] S. Sanyal, S. Hossain , S. Dhar and A. Sanyal, "Computer-aided analysis of saturation in synchronous machines," *MATHEMATICAL MODELLING OF ENGINEERING PROBLEMS,* vol. 4, pp. 95-99, 2017.

[11] D. Pejovski, B. Velkovski and K. Najdenkoski, "MATLAB Model for Visualization of PQ diagram of a Synchronous Generator," in *IEEESTEC - 9th International Students Project Conference*, Nish, 2016.

[12] D. Esmaeil Moghadam, A. Shiri, S. Sadr and D. A. Khaburi, “A practical method for calculation of over-excited region in the synchronous generator capability curves,” in *2014 IEEE 23rd International Symposium on Industrial Electronics (ISIE)*, 2014.

[13] J. Agee, “Maximizing benefits of temporary generator overexcited capability: a special technical session on new operating concepts,” in *2001 IEEE Power Engineering Society Winter Meeting*, 2001.

[14] P. Kundur, J. Paserba, V. Ajjarapu, G. Andersson, A. Bose, C. Canizares, N. Hatziargyriou, D. Hill, A. Stankovic, C. Taylor, T. Van Cutsem and V. Vittal, “Definition and classification of power system stability IEEE/CIGRE joint task force on stability terms and definitions,” *IEEE Transactions on Power Systems,* vol. 19, pp. 1387-1401, 2004.

[15] T. Van Cutsem, “Voltage instability: Phenomena, countermeasures, and analysis methods,” *Proceedings of the IEEE,* vol. 88, pp. 208 - 227, 2000.

[16] A. J. Wood, B. F. Wollenberg and B. S. Gerald , Power Generation, Operation, and Control, 3rd Edition, Wiley, 2013.

[17] D. Aeggegn, A. Salau and Y. Gebru, “Load flow and contingency analysis for transmission line outage,” *Archives of Electrical Engineering,* vol. 69, pp. 581-594, 2020.

[18] I. Ilić, Z. Maljković, I. Gašparac, M. Pavlica, D. Ilić-Zubović, V. Jarić, A. Višković and R. Belobrajić, “METHODOLOGY FOR DETERMINING THE ACTUAL PQ DIAGRAM OF A HYDROGWENERATORS,” *Journal of Energy : Energija,* vol. 56, 2007.

[19] F. Milano, Power System Analysis Toolbox Documentation for PSAT version 2.0.0, 2008.

[20] P. Anderson and A. Fouad, Power system control and stability, The Iowa State University Press, 1997.

[21] N. Hashim, N. Hamzah, M. Latip and . A. Sallehhudin, “Transient Stability Analysis of the IEEE 14-Bus Test System Using Dynamic Computation for Power Systems (DCPS),” in *2012 Third International Conference on Intelligent Systems Modelling and Simulation*, 2012.

[22] S. Robak, J. Machowski and K. Gryszpanowicz, “Contingency selection for power system stability analysis,” in *2017 18th International Scientific Conference on Electric Power Engineering (EPE)*, 2017.

[23] “MATLAB App Designer,” MathWorks, [Online]. Available: https://www.mathworks.com/products/matlab/app-designer.html?s_tid=srchtitle_app%20designer_1. [Accessed 15 July 2022].

[24] C.-Y. Lee and M. Tuegeh, “Virtual Visualization of Generator Operation Condition through Generator Capability Curve,” *Energies*, vol. 14, 2021.

[25] J. Dragosavac, Ž. Janda, J. V. Milanović, D. Arnautović and B. Radojičić, “On-line estimation of available generator reactive power for network voltage support,” in *8th Mediterranean Conference on Power Generation, Transmission, Distribution and Energy Conversion (MEDPOWER 2012)*, 2012.

[26] M. Vražić, A. Viskovic and Z. Hanic, “User P-Q Diagram as a Part of a Synchronous Generator Monitoring System,” *Electronics and Electrical Engineering*, vol. 20, pp. 33-38, 2014.

[27] CIGRE, “Modelling of voltage collapse including dynamic phenomena,” cigre, 1993.

[28] P. Khadka, D. Winkler and T. Øyvang, “Online Monitoring of a Synchronous Generator's Capability with MATLAB,” in *SIMS 2019 Västeräs, Sweden, 13-16 August, 2019*, Sweden, 2020.

[29] M. Adibi and D. Milanicz, “Reactive capability limitation of synchronous machines,” *IEEE Transactions on Power Systems*, vol. 9, pp. 29-40, 1994.

[30] M. Adibi, D. Milanicz and T. Volkmann, “Optimizing generator reactive power resources,” *IEEE Transactions on Power Systems*, vol. 14, pp. 319-326, 1999.

[31] M. Kanjilal, A. K. Patra, J. K. Das and K. Das (Bhattacharya), “Coordination of Loss of Excitation with Capability Curve and Steady State Stability Limit for a Large Alternator,” *International Journal of Electrical Engineering*, vol. 5, pp. 501-521, 2012.

[32] CIGRE, “GENERATOR ON-LINE OVER AND UNDER EXCITATION ISSUES,” cigre, 2015.

[33] T. Dhadbanjan, L. Jenkins, H. Khincha, G. Yesuratnam and B. Kumar, "Monitoring the effects of on-load tap changing transformers on voltage stability," in *2004 International Conference on Power System Technology, POWERCON 2004*, 2004.

[34] T. Øyvang, J. K. Nøland, G. J. Hegglid and B. Lie, "Online Model-Based Thermal Prediction for Flexible Control of an Air-Cooled Hydrogenerator," *IEEE Transactions on Industrial Electronics*, vol. 66, pp. 6311-6320, 2019.

[35] B. Gao, G. Morison and P. Kundur, "Voltage stability evaluation using modal analysis," *IEEE Transactions on Power Systems*, vol. 7, pp. 1529-1542, 1992.

[36] A. K, J. Thomas and P. Thomas, "Analysis of Impact of Non-Electric Dynamics on a Hydro Generator: A Case Study," in *2018 International Conference on Circuits and Systems in Digital Enterprise*, 2018.

[37] T. Dhadbanjan, L. Jenkins, H. Khincha, G. Yesuratnam and B. Kumar, "Monitoring the effects of on-load tap changing transformers on voltage stability," in *Power System Technology, 2004. PowerCon 2004. 2004 International Conference onVolume: 1*, 2004.

[38] G. L. Landgren, "Extended use of Generator Reactive Capability By a Dual Underexcitation Limiter," *IEEE Transactions on Power Apparatus and Systems*, Vols. PAS-99, pp. 1381-1385, 1980.

[39] Y. Gazen, A. Zarnott, A. Morais, G. Cardoso and A. Oliveira, "New setting of loss of excitation protection in P-Q plan in order to maximize the operation area of the capacity curve of the synchronous machine," in *Proceedings of the Universities Power Engineering Conference*, 2014.

ANNEX A: DATA FOR TEST SYSTEM

Table A-1: IEEE 9 bus test system bus data

Bus Number	Voltage Magnitude(p.u.)	Load MW	Load Mvar	Generator MW	Generator Mvar
Bus1	1.04	0.00	0.00	71.61	0
Bus2	1.025	0	0	163	0
Bus3	1.025	0.00	0	85	0
Bus4	1	0.00	0	0	0
Bus5	1	125.00	50	0	0
Bus6	1	90.00	30.0	0	0
Bus7	1	0	0	0	0
Bus8	1	100	35	0	0
Bus9	1	0.0	0	0	0

Table A-2: IEEE 9 bus test system line data

From Bus	To Bus	Resistance(p.u.)	Reactance(p.u.)	Suseptance(p.u.)
2	7	0	0.0625	0
1	4	0	0.0576	0
3	9	0	0.0586	0
4	6	0.017	0.092	0.079
4	5	0.01	0.085	0.088
5	7	0.032	0.161	0.163
6	9	0.039	0.17	0.179
9	8	0.0119	0.1008	0.1045
8	7	0.0085	0.072	0.0745

Table A-3: IEEE 14 bus test system bus data

Bus Number	Voltage Magnitude (p.u.)	Load MW	Load Mvar	Generator MW	Generator Mvar
Bus1	1.06	0	0	0	0
Bus2	1.045	0	0	18.3	5.857
Bus3	1	119	8.762	0	0
Bus4	1	47.79	3.9	0	0
Bus5	1	7.599	1.599	0	0
Bus6	1.07	0	0	11.2	44.2
Bus7	1	0	0	0	0
Bus8	1	0	12.9	0	0
Bus9	1	29.5	16.6	0	0
Bus10	1	9	5.799	0	0
Bus11	1	3.501	1.8	0	0
Bus12	1	6.099	1.599	0	0
Bus13	1	13.5	5.799	0	0
Bus14	1	14.9	5.001	0	0

Table A-4: IEEE 14 bus test system line data

From Bus	To Bus	Resistance(p.u.)	Reactance(p.u.)	Suseptance(p.u.)
1	2	0.01938	0.05917	0.0528
1	5	0.05403	0.22304	0.0492
2	3	0.04699	0.19797	0.0438
2	4	0.05811	0.17632	0.0374
2	5	0.05695	0.17388	0.0339
3	4	0.06701	0.17103	0.0346
4	5	0.01335	0.04211	0.0128
4	7	0	0.20912	0
4	9	0	0.55618	0
5	6	0	0.25202	0

6	11	0.09498	0.1989	0
6	12	0.12291	0.25581	0
6	13	0.06615	0.13027	0
7	8	0	0.17615	0
7	9	0	0.11001	0
9	10	0.03181	0.0845	0
9	14	0.12711	0.27038	0
10	11	0.08205	0.19207	0
12	13	0.22092	0.19988	0
13	14	0.17003	0.34802	0

ANNEX B: MATLAB CODE FOR O.C.C

```
%%Data

Xq_pu=0.6

Xp_pu=0.18

Xd_pu=0.8



n=9

C=0.085

k=1.61

V=0:0.01:1.5

If=(V+C.*V.^n).*k

xad=Xd_pu - Xp_pu

Ep=xad*If



figure (1)

clf

plot (If , Ep, 'b','Linewidth',1.5), hold on

plot (If ,V,'g','Linewidth',1.5)

plot([0 4],[0.8 0.8],'Linewidth',1)

plot([1.615 1.615],[0 2],'Linewidth',1)
```

```
plot([2.63 2.63],[0 2],'Linewidth',1)

plot([1.74 1.74],[0 2],'Linewidth',1)

plot([0 4],[1.2 1.2],'Linewidth',1)

plot([0 4],[1 1],'Linewidth',1)

plot([1.92 1.92],[0 2],'Linewidth',1)

xlabel('If','fontsize',12,'fontname','Times New Roman')

ylabel('Vt','fontsize',12,'fontname','Times New Roman')

legend('Air-gap line', 'Saturation Curve', 'fontsize',12,'fontname','Times New Roman')

axis ([0 4 0 2])
```

ANNEX C: MATLAB CODE FOR SATURATION CALCULATION

```
% data input

%rated quantities for HG1

Sn=160*10^6;

Ua_pu=1;

cosphi =0.95;

Pn=Sn*cosphi/Sn;

PHIn=acosd(Pn/1);

Qn=(Sn*sind(PHIn))/Sn;

Vn=15.8*10^3;

V=1;

Xd_pu=0.8;

Xq_pu= 0.6;

%Potier reactance and armature resistance

Xp_pu= 0.18;

Ra=0.00232;

%Nominal induced voltage

Egn=1.2498;

eq=0:0.1:1

%%Calculation of delta
```

```
%%derivate P in regard to delta to get the maximum delta

a=(eq.*Xq_pu)./(V.*(Xd_pu-Xq_pu))

b=sqrt(a.^2+8)

cosdelta =(1/4).*(-a+b)

del=acosd(cosdelta)

delta=max(del)


%%Calculate the active power and reactive power

%%with eq ranging from 0-1 and use max delta

c=(eq.*V)/(Xd_pu).*sind(delta)

d=(0.5*V.^2).*((Xd_pu-Xq_pu)./Xd_pu*Xq_pu)*sind(2*delta)

P=c+d

P=max(P)

e=2*d

f=((V.^2)./Xd_pu)

Q=((eq.*V)./Xd_pu).*cosd(delta)-f-e

Q=max(Q)


%Rated armature current and terminal voltage

Ian=1;
```

```
Uan=1;

% %Saturation calculation

Sg1=0.077 %%from curve and calculation

Sg12=0.3697 %%from curve and calculation

%%Calculation of Bsat and Asat:

Asat=(Sg1^2)/(1.2*Sg12);

Bsat=5*log((1.2*Sg12)/Sg1);


S_fac=Asat*exp(Bsat*(Egn-0.468));

Ifn=Egn


%%armature current calculations

S=abs(sqrt((P.^2)+Q.^2));

Ia_pu=S./1;

PHI=atand(Q./P);

Ia_pu


%%field current calculations

A=Xq_pu.*Ia_pu.*cosd(PHI) ;

B=Ra.*Ia_pu.*sind(PHI);
```

```
C=Ra.*Ia_pu.*cosd(PHI);

D=Xq_pu.*Ia_pu.*sind (PHI);

delta=atand((A-B)./(Ua_pu+C+D));



E=Xp_pu.*Ia_pu.*cosd(PHI);

F=Ra.*Ia_pu.*sind(PHI);

G=Ra.*Ia_pu.*cosd(PHI);

H=Xp_pu.*Ia_pu.*sind (PHI);

phiportier = atand((E-F)./(Ua_pu+G+H));



%%induced voltage and portier effective value

Eg=Ua_pu.*cosd(delta)+(Ra.*Ia_pu.*cosd(PHI+delta))+Xd_pu.*Ia_pu.*sind(PHI+de
lta);

Ep=Ua_pu.*cosd(PHI)-
(Ra.*Ia_pu.*cosd(PHI+phiportier))+Xp_pu.*Ia_pu.*sind(PHI+phiportier);



hj=1;

%%S_fac=1;

L_row=size(Eg,1);

L_col=size(Eg,2);
```

```
%%S_fac=zeros(L_row,1);

for i=drange(1,L_row)

for s=drange(1,L_col)

if 0.0<=Eg(i,s) && (Eg(i,s)<=1.8)

S_fac(i,s)=Asat*exp(hj.*Bsat.*(Eg(i,s)-0.468));

else

S_fac(i,s)=1;

end

end

end


%%calculation of the armature reaction reactance with Saturation.

Xad_sat=(Xd_pu-Xp_pu)./S_fac;

Xd_pu_sat=Xad_sat+Xp_pu;

% The induced voltage including saturation

Eg_sat=Ua_pu.*cos(delta)+(Ra.*Ia_pu.*cosd(PHI+delta))+Xd_pu_sat.*Ia_pu.*sind(
PHI+delta);

% The field current including saturation

If=Eg_sat./Xad_sat;

If_pu=If
```

ANNEX D: MATLAB CODE FOR CAPABILITY CURVE

```
%% Data Inputs for Salient Pole Rotor Capability Curve

%% Parameter Definition


Sn = 1;                % Rated apparent power [P.U.]

PF = 0.95;             % Power Factor

V = 1;                 % Terminal Voltage (+-5% Voltage Variation if required) [P.U.]

Ia1 = Sn./V;           % Nominal Current [P.U.]

Xd_pu = 0.8;           % Reactance d-axis

Xq_pu = 0.6;           % Reactance q-axis

psi = acosd(PF);       % Power factor angle

%% P: Active Power

%% Q: Reactive Power

%% E01: Induced voltage in stator windings

%% psi: Power factor angle

%% delta: Load angle


Plimit=PF;

Qlimit=sind(psi);
```

```
%Practical stability limit settings

eq=-0.10:0.01:1.0;

i=j;

a=(eq.*Xq_pu)./(V.*(Xd_pu-Xq_pu))

b=sqrt(a.^2+8)

cosdelta =(1/4).*(-a+b)

delta=acosd(cosdelta)

%Active and Reactive Power

c=(eq.*V)/(Xd_pu).* sind(delta)

d=(0.5*V.^2).*((Xd_pu-Xq_pu)./Xd_pu*Xq_pu)*sind (2*delta)

P=c+d

e=2*d

f=((V.^2)./Xd_pu)

Q=((eq.*V)./Xd_pu).*cosd(delta)-f-e

stabm=0.9;

S=(i*Q+P).*stabm;

x_p=imag(S);

y_p=real(S);



%Turbine Power limit settings
```

```
pmax=0.95

%%delta=max(delta)

%% Armature Current Limit

theta=0:0.001:180;

Qx=Sn*cosd(theta);

Py=Sn*sind(theta);



%% Field Current Limit

%%E01=(V*cosd(delta))+(Xd_pu*Ia1*sind(psi+delta));

Emax=1 %%E01

Emin=0.2*Emax



%% Small Pascal Curve Limit

A_x=-V.^2/Xq_pu;

B_x=-V.^2/Xd_pu;



%%small circle E=0

E0=0.0

th1 = (0:0.1:180);

R=(0.5*(V^2)*(Xd_pu-Xq_pu))./(Xd_pu.*Xq_pu)+E0
```

```
c=(0.5*(V^2)*(Xd_pu+Xq_pu))./(Xd_pu.*Xq_pu)-E0

x1= R*cosd(th1)-c;

y1= R*sind(th1);


%%small circle E=0.1

E1=0.1

th1 = (0:0.1:180);

R=(0.5*(V^2)*(Xd_pu-Xq_pu))./(Xd_pu.*Xq_pu)+E1

c=(0.5*(V^2)*(Xd_pu+Xq_pu))./(Xd_pu .*Xq_pu)-E1

x1_01= R*cosd(th1)-c;

y1_01= R*sind(th1);


%%small circle E=0.2

E2=0.2

th1 = (0:0.1:180);

R=(0.5*(V^2)*(Xd_pu-Xq_pu))./(Xd_pu.*Xq_pu)+E2

c=(0.5*(V^2)*(Xd_pu+Xq_pu))./(Xd_pu.*Xq_pu)-E2

x1_02=R*cosd(th1)-c;

y1_02=R*sind(th1);
```

```
th2 = (0:0.1:51.5);

R=(0.5*(V^2)*(Xd_pu-Xq_pu))./(Xd_pu.*Xq_pu)+Em1

c=((0.5*(V^2))*(Xd_pu+Xq_pu))./(Xd_pu .*Xq_pu)-Em1

x2= R*cosd(th2)-c;

y2= R*sind(th2);


th2 = (64.5:0.1:90);

m2=Qlimit

m1=A_x

n2=Plimit

n1=0

R=sqrt((m2-m1).^2+(n2-n1).^2)


y3= R*cosd(th2)%%-c;

x3= R*sind(th2)+A_x;


%%Capability Diagram limits plot

figure (1)

clf

%%Armature current plot settings
```

```
plot(Qx,Py, 'b', 'linewidth',2.5), hold on %Armature current limit plot

%%Field current plot settings

plot(x2,y2, 'm', 'linewidth',2.5), hold on %Field current limit plot

plot(x3,y3, 'r', 'linewidth',2.5), hold on %Field current limit plot

%%Maximum power limit settings

plot([-1 1],[PF PF], 'y', 'linewidth', 2.5) %%Pmax/Turbine Limit

%%Small psacal curve settings

plot (A_x, 0, 'o','linewidth', 1.5 )

plot (B_x, 0, 'o', 'linewidth', 1.5)

%%Practical Stability Limit

plot(x_p, y_p, 'k', 'linewidth',1.5)

%%small circle E=0 curve settings

plot (x1, y1, 'g','linewidth', 1.5 ) %%first semi-circle

plot (x1_01, y1_01, 'b','linewidth', 1.5 ) %%second semi-circle

plot (x1_02, y1_02, 'm','linewidth', 1.5 ) %%second semi-circle

%%plot (x2_01, y2_01, 'b','linewidth', 1.5 ) %%second semi-circle

plot([A_x Qlimit],[0 Plimit], 'linewidth',2) %%Line from A_x to Pmax

plot([0 Qlimit],[0 PF], 'Linewidth',2.5) %%Sn

plot([0 0],[0 -1.346],'w','linewidth',2) %%origoaxis
```

```
%% Chart


SemiCircleR = 0.2:0.2:1.8;

phi = linspace(0, pi, 100);


CirX = @(phi,r) r.*cos(phi);

CirY = @(phi,r) r.*sin(phi);


for rr = SemiCircleR

   plot(CirX(phi, rr), CirY(phi, rr), 'color',[0.4, 0.4, 0.4]);

   hold on

end


PhiList = asin([0.1,0.2, 0.3, 0.4, 0.5, 0.6, 0.7, ...

            0.75, 0.8, 0.85, 0.9, 0.95]);


rr = linspace(0.2, 1.8, 100);


for ii = 1:length(PhiList)

   plot(CirX(PhiList(ii), rr), CirY(PhiList(ii), rr), 'color',[0.4, 0.4, 0.4]);
```

```
    hold on
end
for ii = 1:length(PhiList)
    plot(-CirX(PhiList(ii), rr), CirY(PhiList(ii), rr), 'color',[0.4, 0.4, 0.4]);
    hold on
end


% Numbers
R_tags = [ 0.2,0.4,0.6,0.8,1.0,1.2,1.4,1.6,1.8];
PF_tags = [0.2,0.4,0.6,0.7,0.75,0.8,0.85,0.9,0.95];


hT = text(-0.02, -0.03, '0.0');
set(hT, 'fontweight','bold','fontsize',12);
for ii = 1:length(R_tags)
    s1 = sprintf('%0.1f', R_tags(ii));
    hT = text(R_tags(ii)-0.03,-0.03, s1);
    set(hT, 'fontweight','normal','fontsize',10);
    hT = text(-R_tags(ii)-0.03,-0.03, s1);
    set(hT, 'fontweight','normal','fontsize',10);
    hT = text(0.01,R_tags(ii)+0.03, s1);
```

```
    set(hT, 'fontweight','normal','fontsize',10);
end

Mt1 = [0,0,0,0,0,0.01,0.01,0.01,0.01];
Mt2 = [0,0,-0.03,-0.03,-0.02,-0.02,-0.02,-0.01,-0.015];
Mr2 = [0,-0.01,-0.01,-0.02,-0.02,-0.03,-0.03,-0.04,-0.05];

for jj = 1:length(PF_tags)
    s2 = sprintf('%0.2f', PF_tags(jj));
    pf0 = PF_tags(jj) + Mt1(jj);
    r0 = 1.86;
    hT = text(r0*(1- pf0^2)^0.5, r0*pf0, s2);
    set(hT, 'fontweight','bold','fontsize',12);
    pf0 = PF_tags(jj) + Mt2(jj);
    r0 = 1.95 + Mr2(jj);
    hT = text(-r0*(1- pf0^2)^0.5, r0*pf0, s2);
    set(hT, 'fontweight','bold','fontsize',12);
end

set(gcf, 'Unit','normalized','Position',[0,0,1,1])
```

```
set(gca,'visible','off')

set(gcf, 'color','w');


plot([-1.9 1.9],[0 0],'k', 'LineWidth',2); hold on

plot([0 0],[0 1.9],'k','LineWidth',2.2);


hT = text(1.9, -0.04, 'Q [P.U.]','fontname','Times New Roman');

set(hT, 'fontweight','bold','fontsize',12);

hT = text(0.02, 1.90, 'P [P.U.]','fontname','Times New Roman');

set(hT, 'fontweight','bold','fontsize',12);


axis equal;


hT = text(-0.98,2.0,'Salient Pole Synchronous Generator Capability Curve','fontname','Times New Roman');

set(hT, 'FontSize', 14, 'FontWeight','Bold');


legend('Armature Heating Limit','Min Excitation Limit','Field Heating Limit','Turbine Power Limit','Ax','Bx','Practical Stability Limit','fontname','Times New Roman')
```

ORIGINALITY REPORT

report

ORIGINALITY REPORT

9%
SIMILARITY INDEX

PRIMARY SOURCES

1	ntnuopen.ntnu.no Internet	123 words — 1%
2	S. Patel, K. Stephan, M. Bajpai, R. Das et al. "Performance of Generator protection during major system disturbances", IEEE Transactions on Power Delivery, 2004 Crossref	58 words — < 1%
3	apps.dtic.mil Internet	57 words — < 1%
4	Arnautovic, D., Z. Janda, J.V. Milanovic, J. Dragosavac, and B. Radojicic. "On-line Estimation of Available Generator Reactive Power for Network Voltage Support", 8th Mediterranean Conference on Power Generation Transmission Distribution and Energy Conversion (MEDPOWER 2012), 2012. Crossref	44 words — < 1%
5	vdocument.in Internet	35 words — < 1%
6	bibliotekanauki.pl Internet	34 words — < 1%
7	Adjoudj, Labiba, Fatiha Lakdja, Fatima Zohra Gherbi, and Djaffar Ould Abdsallem. "Synthesis	29 words — < 1%